Utrecht University

SRON
Netherlands Institute for Space Research

Bachelor Thesis

A comparative analysis of disruptive type-I X-ray bursts with non-monotonic decays

January 18, 2017

Author:
Maarten Kries
Physics and Astronomy
Utrecht University

Supervisor:
Dr. Jean in 't Zand
SRON

UU-contact:
Prof. Dr. Cristiane de Morais Smith
Utrecht University

Abstract

Previously, only 5 type-I X-ray bursts with variability in the burst decay were known. During a systematic search through the archive of automatically observed triggers of the Swift X-ray observatory, 3 additional bursts were found that show strong variability (∼70% amplitude), making a total of 8 bursts that show this behaviour. 4 bursts that were observed with Swift (one of which was already known to show variability) are discussed in detail and compared with 4 previously known bursts. We find many similarities. They are likely all ultra compact X-ray binaries, the bursts are all intermediate duration bursts and probably have superexpansion. We speculate that the fluctuations and eclipse-like features are caused by a resettling accretion disk that was disrupted by the effects of super-Eddington fluxes, including an expanding shell and a strong radiation pressure.

Keywords. accretion, accretion disks – X-rays: binaries – X-rays: bursts – X-rays: individual (4U 1850-087, Swift J1734.5-3027, IGR J17062-6143, SAX J1712.6-3739)

Title page image: Artist's concept of a superburst on the surface of a neutron star, disturbing the surrounding accretion disk. Source: `https://www.nasa.gov/centers/goddard/news/topstory/2004/0220stardisk.html`

Contents

Chapter 1

Introduction

1.1 Neutron stars

Neutron stars (NSs) and black holes (BHs) are the remnants of stars with initial masses in excess of 8 solar masses ($M_\odot$). They are the densest objects in the universe. Typically, NSs have a mass of around 1.4 $M_\odot$ and a radius of the order of 10 km. The magnetic field of a NS is related to its age, with older stars having weaker magnetic fields, though there are exceptions. The field strengths range up to 10^{12-15} G. NSs are the end product of stellar evolution and the formation of isolated NSs is different than the formation of NS in binary systems.

1.1.1 Structure

A NS has five major regions: the inner and outer cores, the crust, the envelope and the atmosphere (see Fig. 1.1). The surface layer of an accreting NS has a composition equal to that of the donor star. This include predominantly hydrogen and/or helium, depending on the donor star. Through nuclear reactions in the surface layer, heavier elements form below the surface layer containing hydrogen and helium (see Fig. 1.2). The envelope is thought to be fluid.

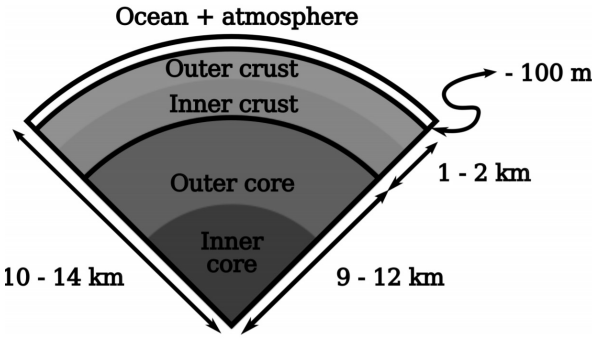

Figure 1.1: Neutron star internal structure. Image from: Cavecchi (2013)

The crust extends to ∼1 km below the surface. This layer contains mostly nuclei

ranging from ^{56}Fe at lower densities to nuclei with a mass number of ∼200 (Lattimer and Prakash, 2004). Much less is known about the core of the NS. The mass of the core can contain as much as 99% of the total NS mass. The outer core consists of a soup of nucleons, electrons and muons. In the inner core exotic particles may become abundant, such as baryons containing a strange quark, also known as hyperons. It is also possible that a transition to a mixed phase of hadronic and deconfined quark matter develops. The energy loss by neutrino emission from the interior is much larger than the energy loss from photons (mainly x-rays) until the star becomes $\sim 3 \times 10^5$ years old.

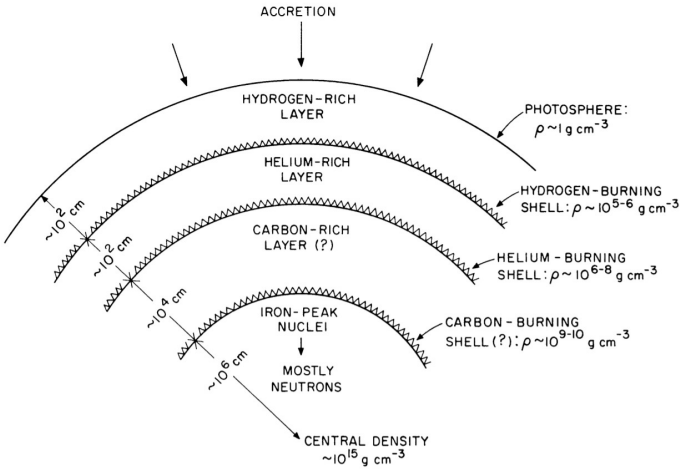

Figure 1.2: Structure of the surface layers of a NS. Image from: Lewin and Joss (1981)

1.1.2 Isolated neutron star formation

A star with M $\geq$ 8 M$_\odot$ ends its life in a supernova explosion. NSs are the remnants of type-II, Ib and Ic supernovae. The explosion is a result of the gravitational collapse of the star's core whose mass has exceeded the Chandrasekhar limit. The currently accepted value of this limit is $\simeq$ 1.39 M$_\odot$ (Hawking and Israel, 1989; Mazzali et al., 2007). If the core mass exceeds this value, the electron degeneracy pressure is no longer sufficient to balance the gravitational force and therefore the core implodes leading to a supernova. The collapse of the core stops when its density reaches the nuclear equilibrium density ($n_0 \simeq 0.16$ fm^{-3}). Infalling matter then rebounds off the core which then causes a shock wave propagating outwards. The core or proto-NS left behind shrinks rapidly because of the pressure loss caused by neutrino emission during this shock wave. This loss of neutrinos forces electrons and protons to combine, making the core neutron-richer, while warming the interior. The temperature doubles to $\sim 6 \times 10^{11}$ K for a short time and then cools through steady emission of neutrinos (Lattimer and Prakash, 2004).

NSs have minimum and maximum mass limits. The maximum mass is of a relativistic origin and lies somewhere between 2.01 $\pm$ 0.04 M$_\odot$ (Antoniadis et al., 2013)

and 3 $M_\odot$. The minimum stable NS mass is about 0.1 $M_\odot$, although a more realistic minimum is $\sim$1 $M_\odot$ (see Lattimer and Prakash, 2004). There is also the possibility that the proto-NS will not survive and collapse into a black hole.

1.1.3 Binary neutron star formation

The evolution of binaries depends on the initial masses and separation of the primary and secondary star. Depending on the properties mentioned above, a high mass X-ray binary (HMXB) or low mass X-ray binary can be formed (LMXB).

HMXBs originate from a binary system with a primary star heavier than the O or B secondary star present in such X-ray binaries (Kutschera, 1998). This heavy star evolves quickly and explodes as a supernova. In general, the binary system can be disrupted by the supernova explosion. If, however, the mass ejected from the system is less than the mass left, the binary binding can survive.

In LMXB systems the masses of donor stars are low and these stars are unevolved. The mass of the primary star progenitor must be high enough to produce a NS. This mass of the primary can exceed the secondary mass by a factor ≥ 20 in the case of ultra compact X-ray binaries (UCXB), where the secondary must have a very small mass (see Seward and Charles, 1995, p.231). The evolution sequence consists of several steps. At first, a common envelope forms due to the short time scale of nuclear evolution of the massive primary. The common envelope is gas enveloping the binary system. During this phase, the hydrogen envelope is dispersed and the binary orbit shrinks. If the primary explodes as a supernova before the envelope is expelled, the system becomes disrupted. After the common envelope phase, the binary system with a helium star emerges.

Alternatively, it is thought that an LMXB can form through an accretion-induced collapse of the white dwarf. In this model, the Chandrasekhar mass white dwarf collapses to a neutron star when some matter is accreted onto it. The progenitor binary consists of two low mass stars, with the heavier one becoming the carbon white dwarf. It remains questionable if this happens in nature since the carbon white dwarf contains a lot of nuclear fuel which can disrupt the star entirely if it ignites.

1.2 Binary systems with neutron stars

HMXBs exist of a NS or a BH and a massive OB-like donor-star. In order for the binary system to be an X-ray binary, matter from the larger star has to be transferred to the compact accretor. In HMXBs this transfer of material is provided by a powerful stellar wind from the high mass star.

LMXBs have a donor star with a mass less than $\sim$ 1 $M_\odot$. They accrete matter due to the low-mass star filling its Roche lobe (Lewin et al., 1993). The Roche lobe is the region around a star in a binary system in which material is gravitationally bound to that star. If a star's surface extends beyond the Roche lobe, then material can be transferred to the compact object through the inner Lagrangian point. The compact object in LMXBs can be a NS or a BH. If the source shows X-ray bursts or pulsations,

then it must be a NS. Finally, if it has a luminous soft X-ray spectrum, then it may be a BH. When the compact object in a binary system is an accreting white dwarf (WD), it is called a cataclysmic variable (CV). These CVs can exhibit dwarf novae and novae, but they are significantly fainter than LMXBs (Seward and Charles, 1995). When an LMXB has an orbital period of less than ∼1.5 hours, the LMXB is classified as an UCXB. UCXBs have a very small orbit which can only fit a very small donor star. The donor star is usually the helium core of a white dwarf from which the outer hydrogen layers are stripped (Nelemans et al., 2009).

1.3 Accretion disks around neutron stars

When the donor star fills its Roche lobe, material can flow through the inner Lagrangian point (Seward and Charles, 1995; Ryden, 2016, see chapter 9 and 10). This point is a saddle point in the equipotential surfaces of the two stars. Through this point, matter can flow to the NS and accrete onto the NS. The mass flowing through the Lagrangian point has angular momentum, which prevents it from flowing directly to the NS. The matter roughly conserves angular momentum and therefore will end up on a circular Kepler orbit around the NS forming a disk. The radius of this orbit is much larger than the radius of the NS. Where the stream of matter coming through the inner Lagrangian point impacts on the disk, a bulge is formed on the accretion disk. For a typical system with a compact object mass of 1 $M_\odot$ and a donor star mass of 0.2 $M_\odot$ having an orbital period of 2 hours, the observed radius of the disk is ~ 0.3 a, where a is the separation of the two stars (Spruit, 2010). The disk is relatively thin, but the inner region of the disk can be dominated by radiation pressure rather than gas pressure. The result of radiation pressure is that the disk becomes thicker near the NS.

Because the accretion disk radiates energy, particles must descend into an orbit with a smaller radius, i.e. into a lower gravitational potential, to conserve energy. To achieve this, these particles must lose angular momentum. The angular momentum in the disk is transferred internally and therefore as these particles spiral inward, other particles must move outward. The result is that the disk is radially broadened. Transfer of angular momentum in the disk happens through the shear flow between neighbouring Kepler orbits in the disk causing friction due to viscosity.

The radiation from the inner parts of the accretion disk has to ionize a large amount of the disk's surface in order to make the disk hot and viscous, so that accretion happens. Therefore, the shape of the disk cannot be flat. The shape of the accretion disk should be thickened as the distance to the NS increases, so that a larger disk surface is illuminated (priv. comm. in 't Zand, 2017).

1.4 Type-I X-ray Bursts from neutron stars

X-ray binaries in which the compact object is a NS can exhibit X-ray bursts. In such a binary system, the NS accretes matter from the donor star. Most of this matter is hydrogen or helium, depending on the composition of the donor star. This ac-

creted matter will form a surface layer on the NS which undergoes nuclear burning (see Fig. 1.2). Hydrogen burns steadily, forming an underlying layer of helium. Eventually the conditions in the helium layer will be appropriate for the ignition of helium. Helium burning is, however, is not a stable process, causing the layer to rapidly burn and producing a thermonuclear flash heating up the photosphere to $\sim 10^7$ K: an X-ray burst. If more time has passed since the last burst, it is likely that more helium is produced which results in a larger burst.

X-ray burst profiles have a few characteristic features: the rise time of the burst is shorter than the decay time, profiles are shorter at higher energies as a result of the surface cooling over time and burst profiles are generally smooth.

Bursts can be classified in two categories: type-I and type-II X-ray bursts. Type-I bursts are the most common type of bursts. These bursts are the result of a normal thermonuclear flash, as mentioned before. Type-II bursts are very uncommon.

The X-ray spectra during bursts are consistent with blackbody emission. Some thermonuclear flashes are powerful enough to expand the photosphere (photospheric radius expansion: PRE), followed by a contraction during which it returns to its original size (Lewin et al., 1993). The photosphere is the visible part of the atmosphere. The X-ray spectrum shows that the radius changes during these burst. This expansion is caused by the luminosity reaching the Eddington limit. The Eddington limit is the maximum luminosity at which the radiation pressure and the gravitational force balance each other. When this limit is surpassed, the atmosphere of the NS starts to expand due to the radiation pressure. The temperature of the photosphere decreases while the radius of the photosphere expands.

When the expansion of the photosphere is large, the temperature may become low enough for the peak of the radiation to shift to UV- (or longer) wavelengths. Little or no X-rays are emitted at this stage. Therefore, the initial peak is separated from the 'main' burst. This is called a 'precursor'. If the burst is less powerful, the burst may have a double peaked profile due to the flux partially being shifted out of the X-ray band. After the expansion, the photosphere contracts and the temperature increases. The moment at which the photosphere returns to the surface of the NS is called 'touchdown', which is characterized by a peak in the blackbody temperature and a dip in the lightcurve. Sometimes the photosphere reaches radii in the order of 10^3 km. Precursors are often seen in this extreme expansion of the photosphere, called superexpansion (in 't Zand and Weinberg, 2010).

1.4.1 More detailed description of the burning process

The composition of the accreted material is important because the burst properties depend on this (Strohmayer and Bildsten, 2003). When hydrogen and helium are accreted onto the NS, the material undergoes hydrostatic compression as new matter continues to be piled up. This mixture typically reaches ignition densities and temperatures within a few hours to days; the wait time depends on the accretion rate per unit area. The temperature exceeds 10^7 K in most of the fuel layer, causing hydrogen to burn via the hot CNO cycle. For high accretion rates (>900 g cm^{-2} s^{-1}) this process is

thermally stable resulting in a pure helium shell. For lower accretion rates the hydrogen burning is thermally unstable and can act as a trigger for type I bursts. For even higher accretion rates ($> 2 \times 10^3$ g cm^{-2} s^{-1}) the ignition conditions for helium are reached before the hydrogen is completely burned, and a mixture of He and H burns during the burst.

Hydrogen burning is a much slower process than helium burning. Therefore, hydrogen rich bursts tend to be longer than helium bursts, ~ 100 s and ~ 10 s respectively. If the accretion rate is sufficiently low (i.e. ~ 0.01 times the Eddington limit), a larger amount of helium can be accumulated. This creates a much thicker layer of helium than normally accumulated between bursts and causes a longer burst. These are called intermediate duration bursts (in't Zand et al., 2005). For pure helium bursts, the fuel burns very rapidly often resulting in exceeding the Eddington limit, leading to Photospheric radius expansion (PRE) bursts. The expanding photosphere leads to a precursor or a double peaked profile in the lightcurve as mentioned before. In the case of bursts with both hydrogen and helium the temperatures reached can produce elements far beyond the iron group via the rapid-proton process. This process starts after the flash heats the gas to high enough temperatures allowing breakout reactions in the nuclear chain starting with the 3α process.

Next to 'normal' and intermediate duration bursts, there is a third classification: superbursts. Superbursts are bursts resulting from thermonuclear flashes occurring in fuel layers at greater depth than 'normal' Type-I X-ray bursts. Precursors are a common feature of superbursts. It is unlikely that unstable helium burning could provide a fluence as large as seen in superbursts. Burning of a large amount of carbon, that is left over from previous bursts, could be the energy source for these superbursts (Strohmayer and Bildsten, 2003).

Bursts from a NS surface may have an effect on the accretion properties. The accretion rate may change during a Type-I burst. For instance, if the flux reaches the Eddington limit the accretion may stop altogether if one assumes isotropic emission from the burst. At lower luminosities this might actually enhance the accretion rate through the Poynting-Robertson drag (Worpel et al., 2013).

Sometimes the lightcurves of bursts show strong fluctuations and/or eclipse-like features during the decay (for example: in't Zand et al., 2011). These are probably due to disturbances in the accretion disk. The disruption of the accretion disk by the blown off photosphere can happen through radiation pressure of the burst or the ram pressure of the ejected gas plowing through the disk in powerful bursts (in't Zand et al., 2011, 2012) (see cover image).

Up to now, only 5 cases have been reported of strong fluctuations during the decay of long type-I X-ray bursts. It is difficult to constrain models with so few cases (note that $\sim$14000 type-I X-ray bursts that have been detected up to now). There is a great need for more data. Therefore, we have initiated a search for additional cases by systematically going through the database of one X-ray observatory with great potential.

1.5 Research questions

In order to enlarge the known amount of cases that have these features we will pursue several research questions in this paper:

1. We start by looking at how many bursts have strong upward and downward flux fluctuations as detected with Swift-XRT. This has not been done before. We do this by going over the entire Swift database.

2. What are the timing characteristics of the fluctuations for the found bursts?

3. What are the spectral characteristics of the fluctuations?

4. What are the differences and commonalities between all case studies, including the literature cases, and what does that imply for the understanding of the phenomenon?

Chapter 2

Instrumentation and data reduction

The Swift spacecraft is a very useful tool to study bursts. Swift monitors a large area of the sky and the combination with its automatic slewing capability makes Swift very efficient for studying bursts. Swift is especially useful for long and uncommon bursts which have a recurrence time of years. One would have to point a narrow field instrument at a single source for a long time in order to observe a rare burst, whereas Swift can monitor a sixth of the sky at the time and is much more efficiently in acquiring data on rare phenomena.

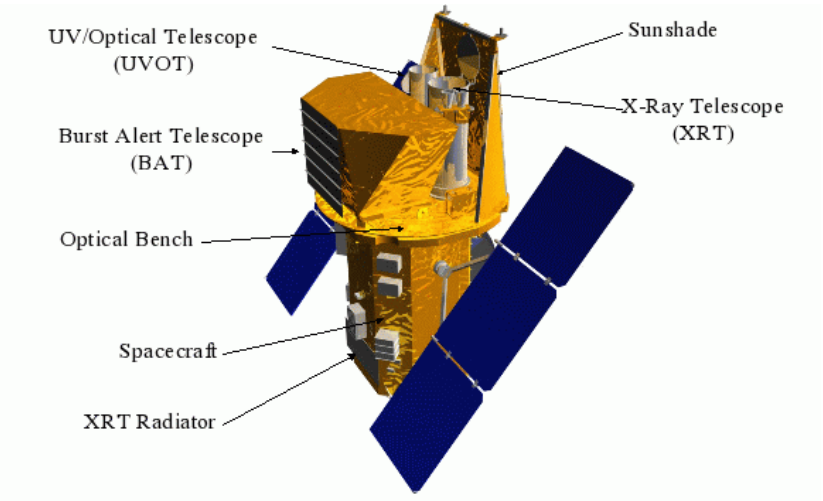

Figure 2.1: Swift spacecraft with its instruments labeled.

2.1 Swift

Swift is a NASA Medium Explorer mission and was launched on the 20$^{\text{th}}$ of November 2004. The main goal of Swift is to search and study Gamma-ray bursts (GRBs).[1] GRBs are the brightest and most energetic events known in the universe, which can

[1]Swift fact sheet: `http://swift.gsfc.nasa.gov/about_swift/Sci_Fact_Sheet.pdf`

last from ~ 0.02 s to several hours. They originate from extremely distant sources and are associated with supernovae explosions and possibly the formation of black holes (for a review, see: Kumar and Zhang, 2015). To observe GRBs and their afterglows, Swift has 3 instruments: the Burst Alert Telescope (BAT, Barthelmy et al., 2005), the X-ray Telescope (XRT, Burrows et al., 2005) and the Ultraviolet/Optical Telescope (UVOT).

The BAT has a large field of view (1.4 sr half-coded and 2.3 sr partially-coded), which is approximately one sixth of the entire sky, in the 15-150 keV energy band. One meter above the detector plane a coded aperture mask is located. This 2.4 m by 1.2 m mask consists of lead tiles in a randomly spread pattern (50% open, 50% closed). This mask allows the BAT to determine the location of a trigger on board to a location accuracy of 1 to 4 arcminutes. Within 12 s of the initial trigger, the BAT has determined the position and calculated the merit after which it may start slewing.

The figure of merit (FoM) is a software module on board Swift which is used to coordinate observations. Every observation has its own merit. When the BAT is triggered, the FoM determines the merit of this trigger and compares it with the merit of the current observation. GRBs always have a high merit, as it is the main goal of Swift to observe them. For Swift to observe an X-ray burst, the merit of the burst must be higher than the merit of the current observation, which can also be a target of opportunity (ToO) uploaded from the ground. If the merit is high enough Swift starts slewing to the source with a maximum slew rate of ~ 50 degrees in 75 s, to pinpoint the XRT and UVOT at the object that was detected with BAT. The average slewing time is $\sim$100 s. The field of view of the XRT is 23.6×23.6 arcmin and 17×17 arcmin for the UVOT. After Swift has slewed towards the source, the XRT and UVOT allow for a much more accurate location measurement of 3 to 5 arcseconds and 0.3 arcseconds, respectively.

In the first five years of the mission, the FoM for known sources (including type-I X-ray bursters, unless not yet known as such) were set to very low values and they would not be observed with the XRT. This has to do with the prime objective of Swift which is observing GRBs. In 2009 this approach changed, a few other targets received higher priority. In 2010 this extended to more targets and bursters with very low bursts rates were allowed to be followed up (C. Markwardt, priv. comm. via in 't Zand). It is from this time on that intermediate duration bursts were followed up.

The XRT uses 12 nested Wolter-I mirrors[2] to focus the X-rays onto a CCD (see Fig. 2.2). Unlike optical light, X-rays cannot be reflected at large incidence angles. The X-rays would just be absorbed by the mirror. X-rays can however be reflected if the incidence angle is very small. A Wolter-I mirror consists of two grazing incidence mirrors that focus X-rays. A single Wolter-I mirror would miss a lot of X-ray photons. Therefore, multiple cylindrical mirrors are nested within each other to focus more photons onto the CCD.[3]

The XRT operates in an auto-exposure mode, which automatically adjusts the

[2] http://www.x-ray-optics.de/index.php/en/types-of-optics/reflecting-optics/curved-mirrors#Wolter_optics

[3] http://imagine.gsfc.nasa.gov/science/toolbox/xray_telescopes2.html

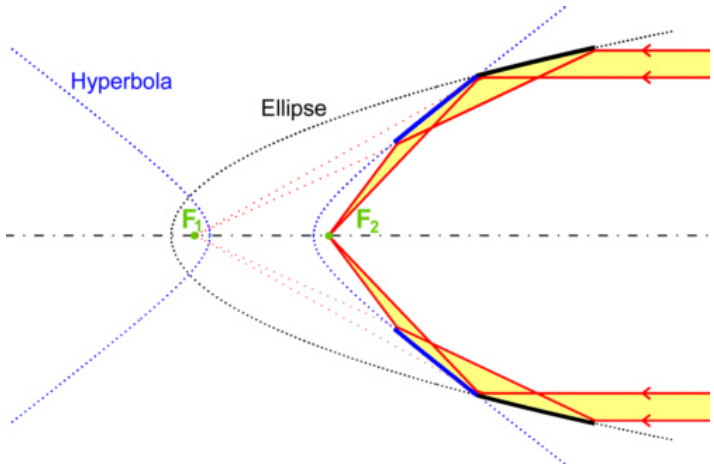

Figure 2.2: Wolter-I mirror configuration. For a distant source (i.e. incoming light parallel to the optical axis) the first mirror is a parabolic mirror instead of an elliptical one.

readout mode of the CCD to optimize the data collection. The CCD collects the position, time and energy of the photons which can be used to measure lightcurves and spectra. The CCD measures 600×600 pixels (2.36 arcseconds/pixel) with a time resolution of 0.14 ms (PD), 1.8 ms (WT) or 0.1 s (IM) / 2.5 s (IM and PC) depending on the readout mode. The energy range of the CCD is 0.2 to 10 keV. The readout modes we used are the windowed timing mode (WT) and the photon-counting (PC) mode. In WT mode, imaging information is only preserved in one dimension and only the central 200 columns (∼8 arcmin) of the CCD are read out. This allows a short time resolution. WT mode is used automatically for fluxes between 600 mCrab and 1 mCrab, but is useful below 5000 mCrab. PC mode on the other hand preserves full imaging which results in a longer time resolution. This mode is used for fluxes below 1 mCrab. To obtain a more uniform point spread function (PSF), the mirror is slightly defocussed.

If 2 photons fall onto a single pixel within one readout time, the energy is added up and if that exceeds a certain threshold the 2 photons are discarded causing a lower observed count rate. One can exclude this so-called 'pile-up' effect by extracting an annular region, ignoring the inner few piled-up pixels and only using the wings of the PSF. For a realistic estimate of the total flux one needs to correct for this pile-up. In WT mode there is generally minimal pile-up below fluxes of 1000 mCrab, but for very bright sources pile-up can occur. The XRT count rates of the bursts we found are all below ∼300 counts s^{-1} and most of the fluctuations do not rise above 200 counts s^{-1}. The XRT pile-up thread from the university of Leicester[4] examines the spectral distortion for 5 different count rate bands depending on the amount of inner pixels excluded. Only one pixel is effected by pile-up between 200 to 300 counts s^{-1}, which is the count rate the bursts discussed in § 3 peak at (∼300 counts s^{-1}). See also § 3.1.3.

[4] `http://www.swift.ac.uk/analysis/xrt/pileup.php`

2.2 Searching bursts with fluctuations

In order to search through the entire Swift database for X-ray bursts we start with the Leicester list of all triggers.[5] This list includes all the GRBs. The search covered all 4400 triggers from 2005-02-23 to 2016-10-07. We removed all the GRBs from the list narrowing it down to 2835 triggers. Then the triggers which noted 'Non burst' were left out, leaving 2469 triggers. Trigger numbers below 00100000 are non-BAT-triggers (such as ToOs). If we exclude all these non-BAT-triggers and the ones who have no object assigned to them, we get a list of 434 triggers.

For the 434 triggers we compared the assigned object names, with the Type-I X-ray burster list from Jean in 't Zand.[6] We also checked if the assigned object names matched one of the aliases of the objects in this burster list. The aliases were retrieved from the Set of Identifications, Measurements, and Bibliography for Astronomical Data (SIMBAD)[7]. 72 triggers have object names which are in the burster list.

Using NASA's ADS ABS[8] search engine we searched through abstracts and titles for papers and Astronomer's Telegrams[9] (ATels) on bursts found by Swift and added them to our list (total 92 triggers). These do include some ToOs and are not BAT-triggered. 32 triggers contained no XRT or UVOT data. This usually happens when the Figure of Merit (FoM) is not sufficient, i.e. an (pre-planned) object is being observed with a higher FoM.

By excluding the triggers which had no object assigned to them, we initially missed the burst from SAX J1712.6-3739 which was found using NASA's ADS ABS, although this burst is triggered by the BAT. Therefore, we also looked through the triggers which did not have an object name assigned to them (2019 triggers). We did not look at trigger numbers 30000 to 39999, which are ToOs uploaded from the ground. 12 triggers matched a known burster in the burster list from J. in 't Zand. 1 trigger had no XRT data, 7 triggers had WT data and 5 triggers had PC data. Except for the trigger from SAX J1712.6-3739, which we already found from papers, none of these triggers showed a burst.

For the ones that had XRT data, we created lightcurves in order to evaluate the data. From this examination we found 10 burst-like lightcurves that were triggered by the BAT. In Table 2.1 we present an overview of these 10 bursts.

To examine the fluctuations in these bursts, we created a script that calculates the running standard deviation of the count rate within a time bin. This is done for different bin times. This value is then compared to the standard deviation expected from Poisson-statistics ($\sqrt{n}$, where n is the mean count rate of the time bin). If the standard deviation is a factor $\geq$2 above the statistically expected Poisson standard deviation, we determine that the fluctuation is significant and may have an origin intrinsic to the source. The found bursts all have standard deviations of $\sim$4 times the Poisson standard deviation. Poisson-statistics are relevant because the data are an

[5] http://www.swift.ac.uk/gcn/index.php#index
[6] https://personal.sron.nl/~jeanz/bursterlist.html
[7] http://simbad.u-strasbg.fr/simbad/
[8] http://adsabs.harvard.edu/abstract_service.html
[9] http://www.astronomerstelegram.org/

event counting process.

Of interest for this paper are only the X-ray bursts which show variations in the decay of the lightcurve. We have found 4 of these bursts from the search: 4U 1850-087, Swift J1734.5-3027, IGR J17062-6143 and SAX J1712.6-3739.

Table 2.1: Overview of the 10 bursts found during the Swift database search, ordered by observation date.

Object	Observation date (UTC) [YYYY-MM-DD HH:MM:SS]	Observation-ID	Instrument	Start XRT-WT (PC) data after BAT-trigger [s]	E-folding time [s]
IGR J00291+5934	2015-07-25 02:12:59	00650221000	BAT+XRT	123 (No PC data)	106
SAX J1808.4-3658	2015-04-11 19:38:41	00637765000	BAT+XRT	52 (No PC data)	53
1RXS J180408.9-342058	2015-02-06 21:01:10	00630047000	BAT+XRT	1160 (No PC data)	57
4U 1850-087	2014-03-10 21:01:40	00591237000	BAT+XRT	691 after start burst	1017 ± 29.8[a]
Swift J1734.5-3027	2013-09-01 09:09:42	00569022000	BAT+XRT	150 after start burst	173.7 ± 3.0
IGR J17062-6143	2012-06-25 22:40:01	00525148000	BAT+XRT	307 after start burst	742.7 ± 30.95
SAX J1712.6-3739	2011-09-26 20:09:28	00504101000	BAT+XRT	241 after start burst	448.8 ± 29.35
H 1820-303/4U1820-30	2009-06-06 09:28:34	00354224000	BAT+XRT	85 (No PC data)	-
H 1820-303/4U1820-30	2009-06-06 09:28:34	00354224001	BAT+XRT	5607 (No PC data)	2.5
1A 1246-588	2006-08-11 03:00:49	00223918000	BAT+XRT	201 (No PC data)	273

[a] see Table 3.6

Chapter 3

Data analysis and results

In this chapter we will first present some general notes about how we extracted the lightcurves, hardness ratios and spectra of the four bursts with fluctuations. Then we will discuss the results of the four bursts individually. We will also argue that these bursts are Eddington limited. We will also discuss four literature bursts that show similar features briefly, after which we will present multiple tables with information and properties of these 8 bursts.

We define 'fluctuations' as the fast variations in flux (up and down) on time scales of tens of seconds, whereas dips are eclipse-like features which only lowers the flux on a longer time scale. Variability is the collective term for both these phenomena.

3.1 General notes

3.1.1 Lightcurves

In the lightcurves the BAT and XRT count rates are plotted with a bin time of 5 s. The BAT trigger times are not necessarily equal to the start time of the bursts. To estimate the burst start time we qualitatively determine where the slope of the BAT lightcurve rise intersects the pre-burst flat level. Start times are not determined very accurately and are estimated within a 10 s uncertainty.

The XRT lightcurves are extracted using a circular region (94.4 arcsec) around the source. We did not filter out the inner few pixels to exclude the pixels where pile-up is most likely to have a noticeable effect (see § 3.1.3).

3.1.2 Hardness ratios

The hardness ratio is the ratio between the count rates in two energy bands. The higher energy band contains the 'hard' X-rays and the lower energy band contains the 'soft' photons. We excluded the inner 2 pixels (4.72 arcsec) while extracting the hardness ratios because pile-up can lead to a hardening of the spectrum which alters the hardness ratio. For all BAT-triggered bursts that we found, we investigated two

hardness ratios and used the same energy bands for all: 2.5 to 10 keV over 0.3 to 2.5 keV and 4.0 to 10 keV over 2.0 to 4.0 keV. We use a bin time of 5 s.

3.1.3 Spectrum

Spectral data below 0.7 keV are ignored as suggested by the Leicester XRT calibration digest[1]. Sources which are heavily absorbed ($N_H > 10^{22}$ cm^{-2}, where N_H is the hydrogen column density of all gas between the observer and the source) can show a 'bump' in the spectra between 0.4 - 1 keV. The energy at which this bump is present changes over years. In 2008 and 2013 it is ~ 0.4 keV and ~ 0.6 keV respectively. It is recommended to exclude data below these energies. The spectra are also background extracted. The background region has a radius of 70.8 arcsec and is located at the edge of the CCD (i.e. far away from the peak of the PSF).

To improve the statistics of the data, i.e. to get higher count rates, we also extracted spectra where we did not filter the XRT data with an annulus but with a circular region around the source. To exclude the effects of pile-up that the resulting data suffers from, one needs to filter out a small region around the peak of the PSF. Pile-up not only has an effect on the lightcurve/count rate but also on the spectrum. If, for example, 2 photons with an energy of 2 keV fall onto the CCD within one readout time, the photon energies are added up to 4 keV. This results in a hardening of the spectrum, i.e. more photons at higher energies and fewer at lower energies. However, this should affect the spectrum as a whole and not a small part of the spectrum like an absorption line. For the purpose of searching narrow spectral features, we think it is, therefore, safe to use a circular region instead of an annulus for the sake of better statistics. For the entire spectra we also used a circle. The use of a circle as region gives us more photons, since a lot of the photons are cut out by extracting the inner few pixels, where the count rate is high. The amount of counts excluded when using an annulus (inner radius of 4.72 arcsec) is: 11 %, 45%, 49% and 41% for 4U 1850-087, Swift J1734.5-3027, IGR J17062-6143 and SAX J1712.6-3739 respectively. This does add an uncertainty to the spectral data.

We grouped the spectrum with the `grppha` tool. The minimum counts per energy channel was set to 20 to allow use of chi-squared as a goodness of fit. The chi-squared statistics are more accurate when there are enough counts in a bin. At larger values of the mean of the Poisson distribution (μ), the Gaussian distribution becomes an acceptable description of the Poisson distribution (see Fig. 2.4 and Fig. 2.5 in Bevington and Robinson, 1992). The probability given in the tables below the spectra is the probability that the observed data are drawn from the model. Spectra were further binned in `XSPEC` but only for plotting aesthetics.

3.1.4 Time resolved spectroscopy

The time resolved spectroscopy is done by analysing spectra in a series of time intervals. In the case of fluctuations we made sure that a number of up/down fluctuation pairs

[1] `http://www.swift.ac.uk/analysis/xrt/digest_cal.php`

fit in the time interval. The bolometric flux is calculated using the `flux` command in `XSPEC` between 0.01 and 40 keV. Before the flux is calculated the absorption (N_H) parameter is set to 0 to get the flux of only the blackbody. The fitted blackbody spectrum is extrapolated to 0.01 - 40 keV (with the `energies` command) which is approximately bolometric for a typical blackbody peak temperature ($\sim$2.5 keV).

3.2 4U 1850-087

3.2.1 General properties

4U 1850-087 (Prodan and Murray, 2015) is a UCXB located in the galactic globular cluster NGC 6712. The distance to the cluster is 6.8 kpc (Peterson and King, 1975; Harris, 1996). It was first detected as an X-ray burster by Swank et al. (1976). The orbital period is 20.6 min, though this has not yet been confirmed. The orbital period could also be 13.2 minutes but this is less likely (see Homer et al., 1996). Homer et al. (1996) derived a secondary mass of 0.04 $M_\odot$ and 0.04 $R_\odot$, under the assumption that the secondary is a fully degenerate helium white dwarf. Prodan and Murray (2015) derive a primary mass of 1.4 $M_\odot$ and suggest that it is a triple system, with a third companion of 0.55 $M_\odot$. From XMM-Newton observations (Sidoli et al., 2005): $N_H = (4 - 6.3) \times 10^{21}$ cm^{-2}. There is evidence for extra absorption in the line of sight, since the best-fit total N_H is always significantly higher than the optically derived value in the direction of the host globular cluster of $(1.8 \pm 0.2) \times 10^{21}$ cm^{-2}. Therefore, the intrinsic absorption ranges from 2 to 4.5×10^{21} cm^{-2}.

3.2.2 Data description/lightcurve

On 10 March 2014, 4U 1850-087 triggered Swift's BAT and slewed in 491 seconds to the source. 691 s after the start of the burst the XRT-WT measurement started. This is relatively long. The measurement lasted around 760 s. In the XRT lightcurve (see Fig. 3.1) we see the decay of a thermonuclear X-ray burst. The start of the burst is approximately 200s before the BAT-trigger time (i.e. The BAT-trigger happened on t=200 s). At the time of the trigger, the count rate had already risen to more than half the peak count rate. The count rate of the BAT data is corrected for the fact that during the slew period, the source is at a changing off axis angle.[2] When the count rate rises, the spectrum becomes harder. The point where the BAT count rate starts to decrease is the touchdown point. After touchdown, the spectrum gradually becomes softer. The touchdown point is the end of the Eddington limited phase (see § 3.2.4).

The XRT lightcurve is from photons within a circular region of 94.4 arcsec around the source. A dip of $\sim$ 20 s long is clearly visible, which is $\sim$ 660 s after the touchdown. Just before and after this dip, the count rate rises. It is possible that there are two wider dips between 1000 - 1200 s and 1300 s onward.

[2] `http://swift.gsfc.nasa.gov/analysis/threads/batfluxunitsthread.html`

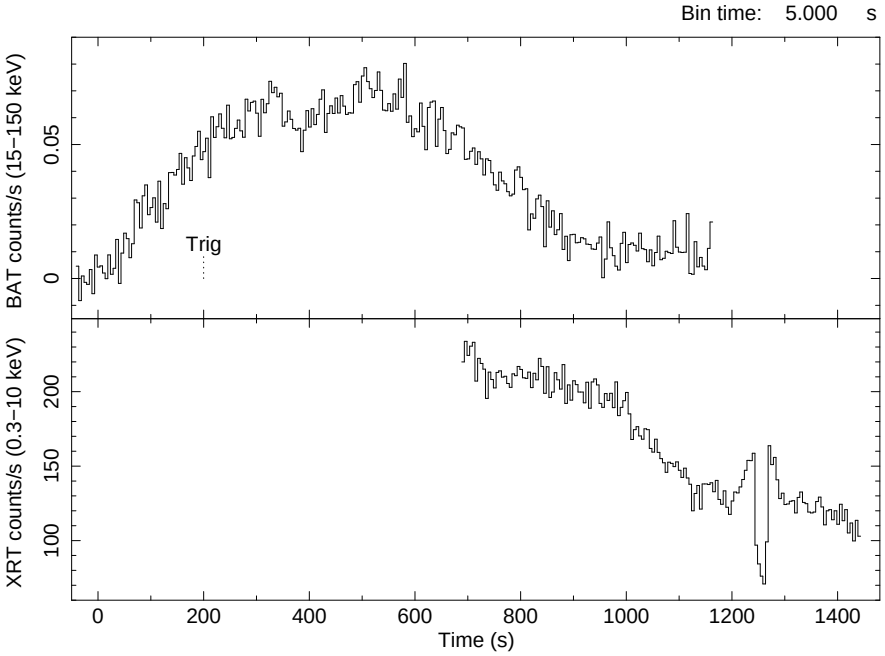

Figure 3.1: **4U 1850-087:** BAT and XRT lightcurves in 5s time bins. The start time (t=0) is set at 56726.876160 MJD. The time at which the BAT triggered on this burst is displayed with a dotted line.

3.2.3 Hardness ratio

The dip at 1250 s after the BAT trigger is also visible in the hardness ratio (2.5-10/0.3-2.5 keV). The hardness ratio (Fig. 3.2) declines as expected from a cooling blackbody. In the hardness ratio (4-10/2-4 keV) the dip is not visible at all.

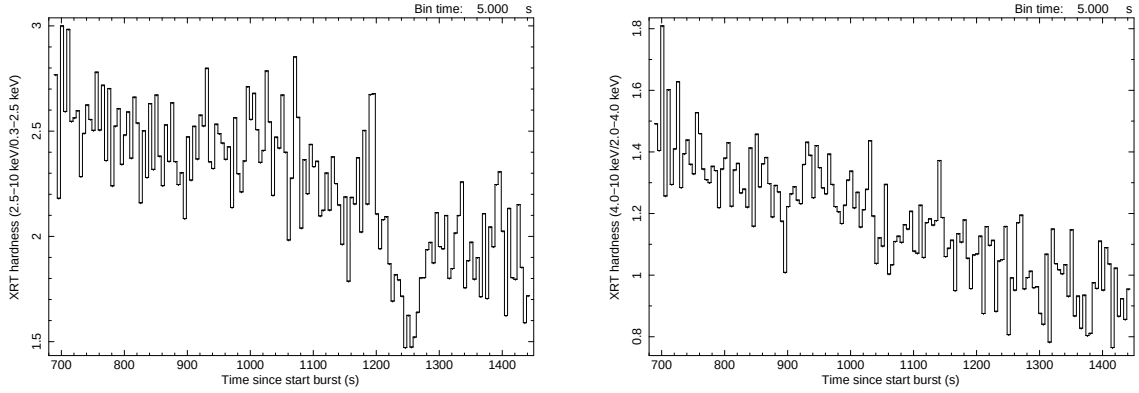

(a) (b)

Figure 3.2: 4U 1850-087: Time profile of 2 hardness ratios.

3.2.4 Eddington limited burst

The BAT lightcurve shows a 'slow' rise of count rate. This slow rise is a feature of PRE (see § 1.4). Due to the expansion of the photosphere in PRE bursts, the peak of the radiation shifts to lower energies leaving no radiation in the energy range of the BAT (see § 3.3). When the photosphere contracts, the peak of the radiation 'slowly' shifts back to higher energies as the temperature rises. This is observed as a slow rise in count rate in the BAT lightcurve. If the burst would not have PRE, the BAT lightcurve would start with a quick rise in count rate and then be followed by a slow decay as the burst cools down.

We also fitted the flat region in the lightcurve with an absorbed blackbody between 2 and 9 keV, with the N_H-value fixed to 0.39×10^{22} cm^{-2} (L. Sidoli 2005). To look at the flux of the blackbody only, we ignored energies below 2 keV since there is much less interstellar absorption above 2 keV. From the extrapolated flux we calculated the bolometric luminosity, assuming the distance to 4U 1850-087 (in cluster NGC6712) to be 6.8 kpc (Harris 1996). A more recent study calculated the distance to be 8 ± 1 kpc, which would result in a higher luminosity (Paltrinieri et al. 2001). The luminosity was 2.2×10^{38} erg s^{-1}, which is around the Eddington limit for hydrogen. This would suggest that the burst luminosity was around or above the Eddington limit for almost 12 minutes, because the count rate was even higher before this 'flat' phase. Because this is after the assumed touchdown point it must be below the Eddington limit. The luminosity is above the Eddington limit for hydrogen which implies that this is a helium burst.

3.2.5 Spectrum

For the time resolved spectroscopy we fitted the spectra with an absorbed blackbody (see Fig. 3.4). The spectrum of the dip and just around the dip (see Fig. 3.3) was fitted with two blackbodies. This gave a better fit than one blackbody. As seen in the burst from IGR J17062-6143 (see § 3.4) a small peak can be seen around 1 keV in the dip spectrum, although less clear.

The persistent emission of 4U 1850-087 as measured with MAXI from 56600 to 56730 MJD stays below approximately 0.02 counts cm^{-2} s^{-1} in both the 2-4 keV and 4-10 keV energy bands, except for the days around the bursts. On average the count rate was $\sim$ 0.01 counts cm^{-2} s^{-1}. Using the NASA `WebPIMMS`[3] tool we estimate the persistent flux (2.0-4.0 keV), which is $\sim 10^{-10}$ erg cm^{-2} s^{-1} for a powerlaw index of 2. The bolometric flux may be a factor $\sim$2 larger. Since we did not model the persistent spectrum we estimated the powerlaw index to be 2. The persistent bolometric flux should therefore be taken with a large uncertainty of 50%. The persistent emission is however, much smaller than the burst emission which was 5.0×10^{-8} erg cm^{-2} s^{-1} at the start of the XRT data. The peak bolometric flux might be a bit higher. Therefore, we did not subtract the persistent emission in the spectra.

[3] `http://heasarc.gsfc.nasa.gov/cgi-bin/Tools/w3pimms/w3pimms.pl`

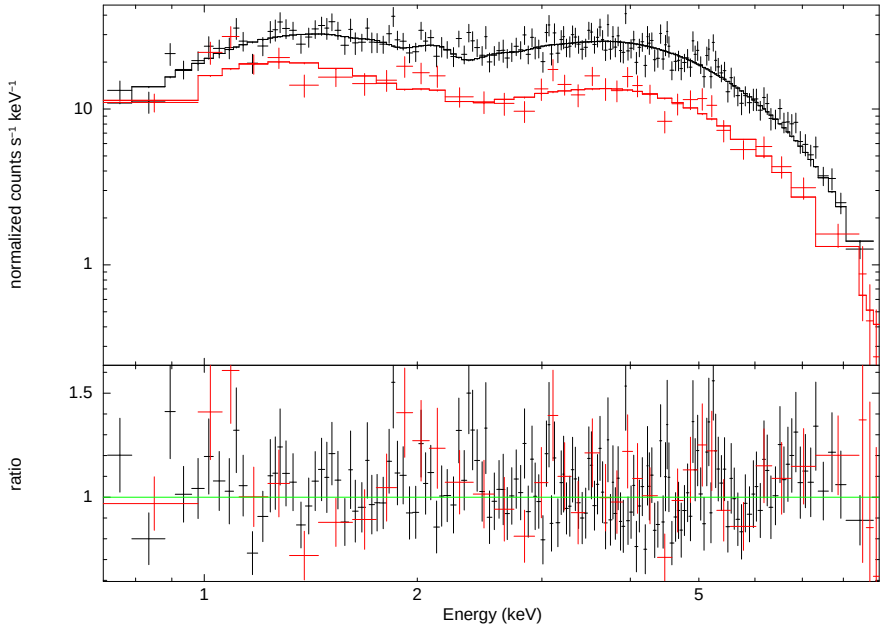

Figure 3.3: **4U 1850-087:** Spectrum of the seconds before and after the dip (black) and the dip (red), modelled with two absorbed blackbodies.

Table 3.1: Spectral parameters for the spectra (Fig. 3.3) during the dip (30 s) and just outside the dip (30 s before and 30 s after). The energies of both blackbodies are linked.

Model component	Parameter (unit)	Inside dip	Outside dip
TBABS	N_H ($\times 10^{22}$)	0.29 fix	0.29 fix
BBODYRAD	kT_{bb} (keV)	0.258 ± 0.021	0.258
BBODYRAD	norm ($\times 10^3$)	12.136 ± 4.816	11.294 ± 4.213
BBODYRAD2	kT_{bb} (keV)	1.9006 ± 0.0385	1.9006
BBODYRAD2	norm	69.793 ± 4.366	151.458 ± 8.212
χ^2_{red}		Fitted same time	0.85811
Null hypothesis probability		Fitted same time	0.98698

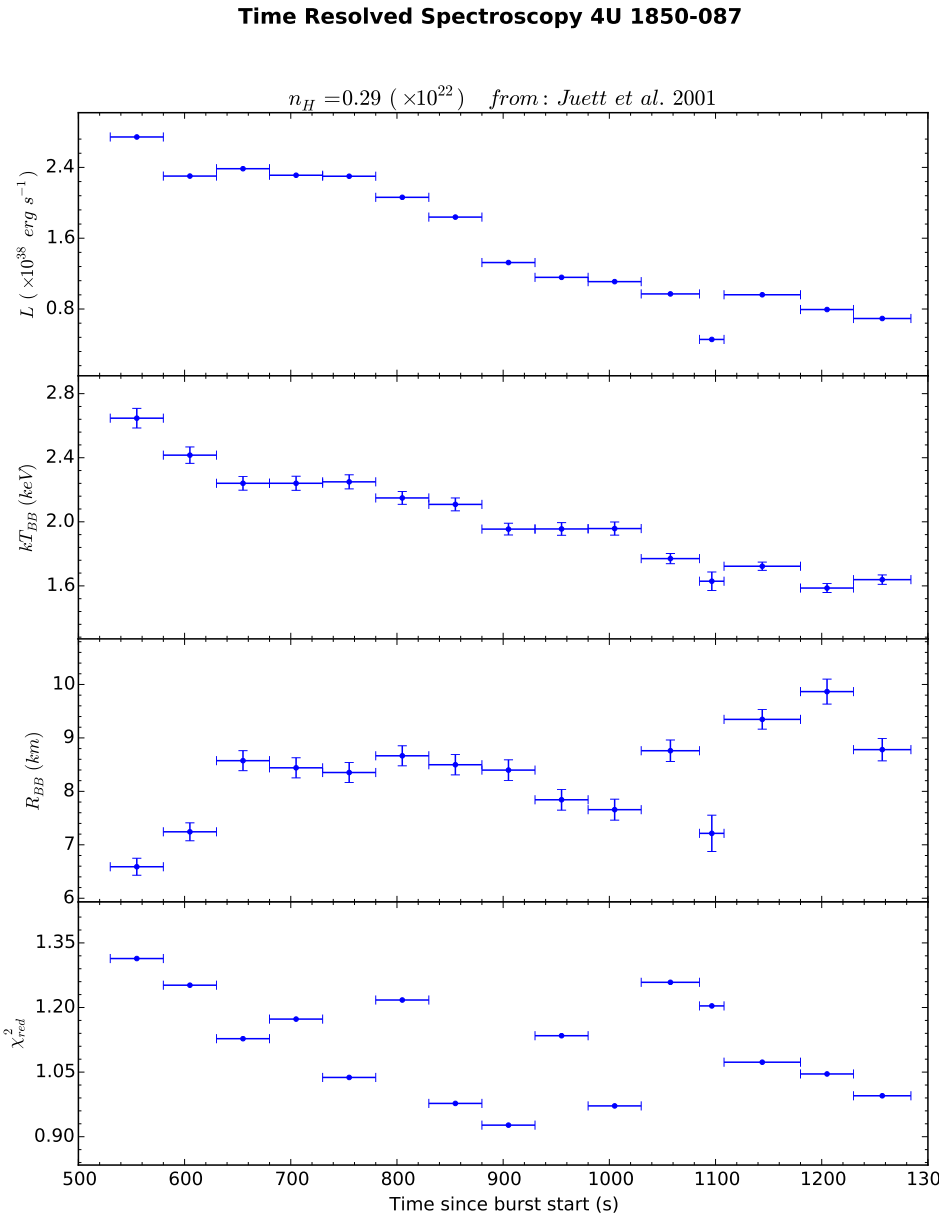

Figure 3.4: **4U 1850-087:** Time resolved spectroscopy for an assumed distance of 6.8 kpc (Prodan and Murray, 2015).

3.3 Swift J1734.5-3027

3.3.1 General properties

Swift J1734.5-3027 is a hard X-ray transient which was discovered by Swift during an outburst on 2013 September 01 (Bozzo et al., 2015). The source underwent an episode of enhanced X-ray activity from May to June that year as seen in archival observations. The transient was classified as a bursting NS LMXB. The BAT lightcurve shows a rise time of $\approx$ 50 s, which is typically observed at the hard X-rays in long Type-I helium bursts with PRE (e.g., Kuulkers et al., 2002; Molkov et al., 2005; Falanga et al., 2008). Bozzo et al. (2015) cannot firmly assess if the burst actually underwent PRE. Assuming PRE happened and an Eddington luminosity for helium of $L_{Edd} \approx 3.8 \times 10^{38}$ erg s^{-1} (Kuulkers et al., 2003), Bozzo et al. (2015) derived a source dinstance of 7.2 ± 1.5 kpc.

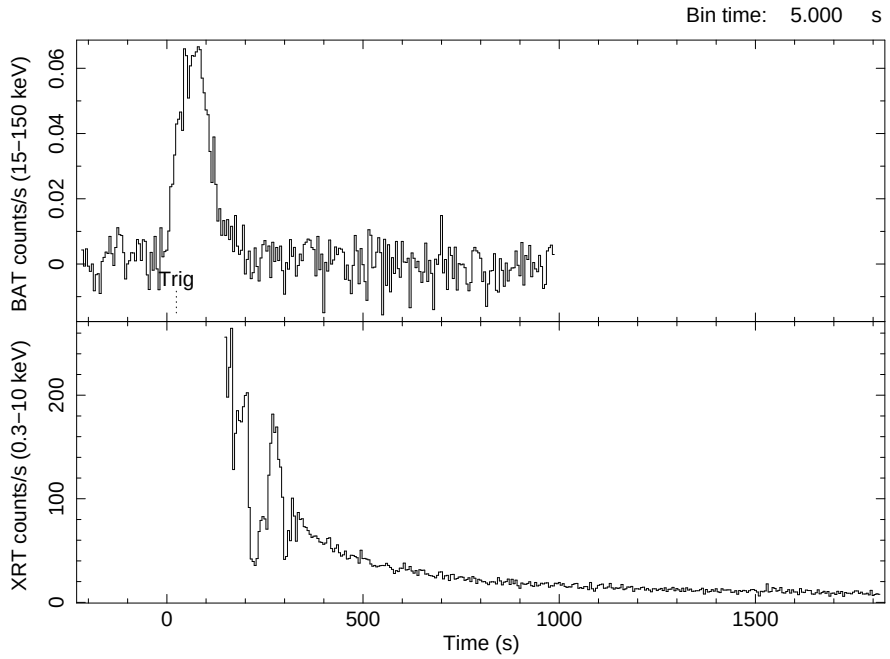

Figure 3.5: **Swift J1734.5-3027:** BAT and XRT lightcurves in 5s time bins. The start time (t=0) is set at 56536.381736 MJD The time at which the BAT triggered on this burst is displayed with a dotted line.

3.3.2 Data description/lightcurve

Fig. 3.5 shows the BAT and XRT light curves. The XRT measurement of the burst lasted for more than 16000 s but only the first 1700 s are a continuous data set. After 1700 s a large 3000 s gap is present and 12 s of data follow. The other 5 bits of data, which are around the same length (12 s), also have big gaps between each other (see Table 3.5, data coverage). There is a little over 1800 s of data in total. The BAT-trigger time is slightly off from the start of the burst, which is approximately 24 s earlier.

The BAT data consist of a short peak with a relatively fast decay time. The XRT lightcurve is obtained through a circular region of 94.4 arcsec around the source. No pixels are cut out to avoid effects of pile-up.

The XRT data start with 2 quick fluctuations followed by 2 longer dips which step up, roughly a third, in count rate halfway the dip. The fluctuations seem to start before the touchdown point, which is estimated to be at 80 s after the start of the burst (see Table 3.6). Due to the shorter duration of the burst, especially in the BAT energy band, the estimated touchdown time is less certain. After these 2 dips, a last short dip can be seen. Bozzo et al. (2015) does not mention fluctuations and dips in the XRT lightcurve. The XRT lightcurve starts 126 s after the BAT trigger.

3.3.3 Hardness ratio

2 hardness curves were created. One for the ratio 2.5-10 keV/0.3-2.5 keV and one for 4-10 keV/2-4 keV. One can clearly see a cooling blackbody in both hardness ratios. As the blackbody cools down, more photons with lower energies and less photons with higher energies are emitted, resulting in a lower ratio of 'hard' photons over 'soft' photons. The first wide dip in the lightcurve, ∼200 s after the start of the burst, coincides with a strong decrease in the hardness ratio (2.5-10/0.3-2.5 keV). After this first wide dip, the hardness ratio first rises before decreasing again. This dip is not seen in the hardness ratio of 4-10/2-4 keV.

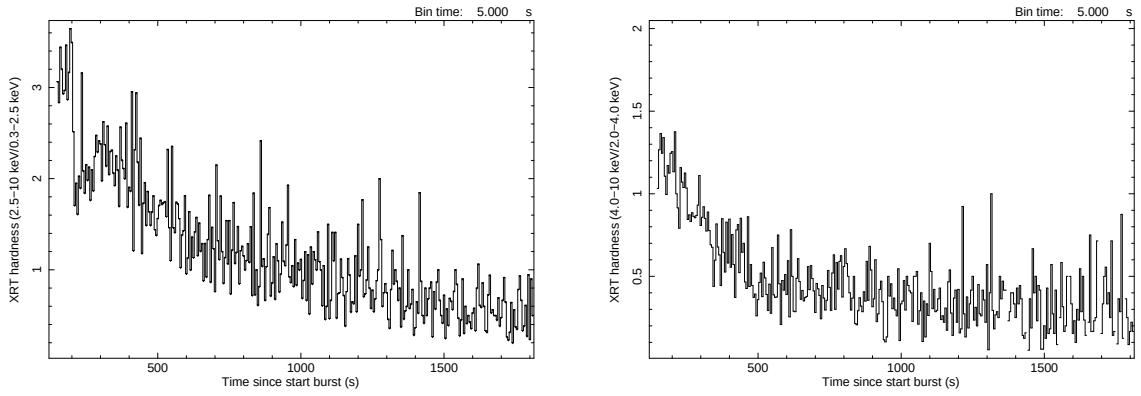

(a) (b)

Figure 3.6: Swift J1734.5-3027: Time profile of 2 hardness ratios.

3.3.4 Eddington limited burst

The BAT lightcurve of Swift J1734.5-3027 is bit shorter than the other 3 bursts. The rise and decay in count rate is quicker, therefore we cannot use the same argument as used in § 3.2.4. Though as argued in Bozzo et al. (2015), we assume that this burst also underwent PRE and that the bursts was, therefore, Eddington limited.

3.3.5 Spectrum

No time resolved spectroscopy was done for this source. See Fig. 4 in Bozzo et al. (2015) for time resolved spectroscopy instead. This source was not found in the MAXI database. Therefore, we assume a low persistent emission (<50 mCrab or $\sim 10^{-9}$ erg cm^{-2} s^{-1}). Bozzo et al. (2015) reported a peak (15-150 keV) flux of $(1.3\pm0.4)\times10^{-8}$ erg cm^{-2} s^{-1}. The bolometric flux is probably higher than this. Therefore, we neglected the persistent emission because it is much lower than the burst emission.

An absorption line at ∼3.8 keV?

Around 3.8-3.9 keV there is an interesting absorption feature seen in the spectrum (Fig. 3.8). This seems most prominent during the first 200 seconds of the XRT data, but can also be seen throughout the data. In order to test the significance of an absorption line in the spectrum of Swift J1734.5-3027, we performed the so-called F-test (Bevington and Robinson, 1992). This gives a measure of the improvement of a new model versus the old model. In this fashion we can add an absorption component to our basic model and determine whether that is a statistically significant improvement. Comparing this with the probability function for 2 degrees of freedom, which is the number of parameters added, we can examine the significance of this particular added component.

We fitted a simple absorbed blackbody to the first 200 s of XRT-WT data. The best-fit gave an χ^2 of 648.15 for 593 Degrees of Freedom (DoF). Then we added a Gaussian absorption line of which we fixed the line width (sigma) to zero. We fixed this to add the least possible parameters to the new model. This model resulted in an χ^2 of 628.11 for 591 DoF. For this added component, F_χ=18.273. This corresponds to a probability of $\sim$ 0.05 of exceeding F for 2 degrees of freedom (see Table C.5 in Bevington and Robinson, 1992). This suggests it is a fairly good addition to the model.

Alternatively, we used a 'BIC'-test or Bayesian information criterion (Kass and Raftery, 1995), which is calculated with the formula: $\chi^2 + k \times \ln n$, where k is the number of parameters of the model and n is the total number of data points. This weighs the decrease in χ^2 against the extra parameter(s). The model with the lowest BIC-value is the one which should be used. For this spectrum, the model without the added GABS component, the BIC-value was 667 versus BIC=660 with the added GABS. The difference is a decrease in BIC-value of $\sim$ 1%. According to Kass and Raftery (1995), a decrease in BIC by 6-10 is strong evidence in favour of the model with the lower BIC-value. According to the BIC-test, the model with an added Gaussian absorption line is preferred over the simpler model.

A check of the background spectrum, which is subtracted in `XSPEC`, showed a peak between 3-4 keV. The count rate of this peak was rather low at 0.2 counts s^{-1} keV^{-1}. The count rate deficiency in the 3.8 keV dip is a little over 20 counts s^{-1} keV^{-1}. Therefore, the background has no significant effect, and cannot be the origin of the absorption since only 1% of the counts is subtracted versus a 10-20% deficiency in the measured spectrum.

To further examine if there is an absorption line around 3.8 keV, we have checked

if this absorption is also seen in other bursts, including GRBs, preferably not much before or after this burst. If this absorption feature is also seen in other bursts, this might indicate an instrumental origin.

- The burst from 4U 1850-087 on 2014-03-10 happened a half year later and showed no significant evidence for an absorption line at ~ 3.8 keV.
- The XRT-data of the automatic trigger 00570069 from Cyg X-2 on 2013-09-08, one week after the burst from Swift J1734.5-3027, showed only very vaguely a sign of a dip in the spectrum around 3.8 keV. Adding an absorption component at 3.85 keV made the fit worse though.
- XRT data collected from H1743-322 on the same day (approximately 4 hours later) also showed some peculiarities around 3.8 keV (see Fig. 3.7).

Considering the points mentioned above, we evaluate the evidence for an absorption feature around 3.8 keV as marginal.

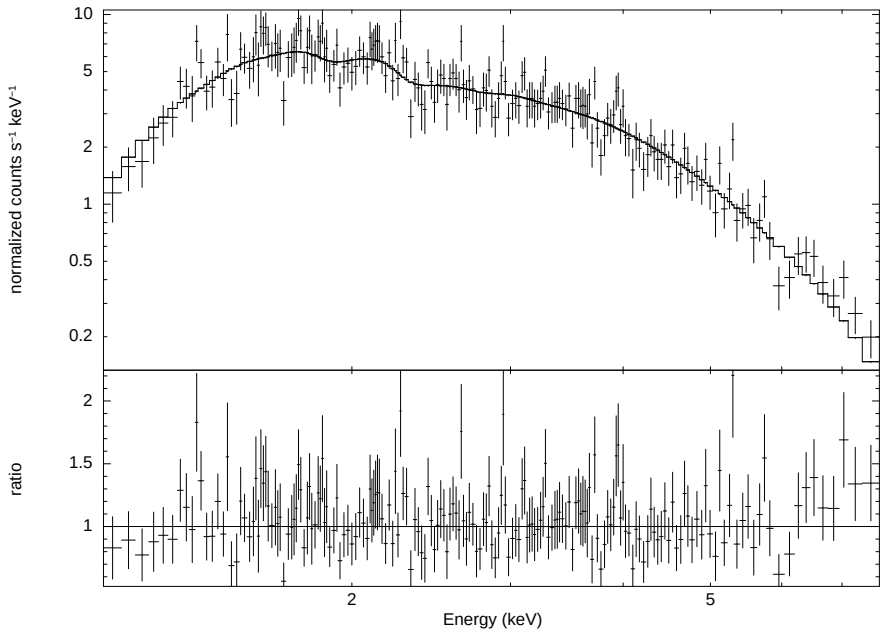

Figure 3.7: **H1743-322:** Spectrum of the observation on the same day of Swift J1734.5-3027. The spectrum is modelled with a single absorbed powerlaw. Note that there is some 'absorption' around 3.8 keV, comparable to that seen in Swift J1734.5-3027. $\chi^2_{red} = 0.98408$, null hypothesis probability=0.548833.

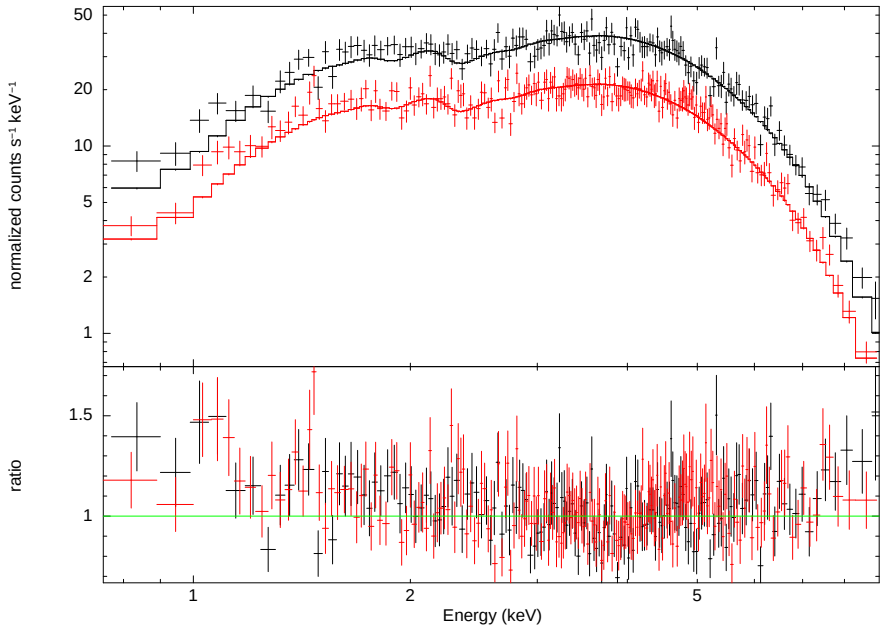

Figure 3.8: **Swift J1734.5-3027:** Spectrum of the first 200 s of XRT data with fluctuations up (black) and down (red), modelled with a single absorbed blackbody.

Table 3.2: Spectral parameters for the spectra of fluctuations up and down. (Fig. 3.8)

Model component	Parameter (unit)	Fluctuations up	Fluctuations down
TBABS	N_H ($\times 10^{22}$)	0.84 fix	0.84 fix
BBODYRAD	kT_{bb} (keV)	1.706 ± 0.024	1.684 ± 0.021
BBODYRAD	norm	214.77 ± 8.19	122.21 ± 4.16
χ^2_{red}		Fitted same time	1.0225
Null hypothesis probability		Fitted same time	0.3177

3.4 IGR J17062-6143

3.4.1 General properties

IGR J17062-6143 was discovered in 2006 as an X-ray source with INTEGRAL (Churazov et al., 2007). It has been active ever since with a luminosity of $L_X \simeq (1-5) \times 10^{35}$ $(\frac{D}{5.0kpc})^2$ erg s^{-1} (Ricci et al., 2008; Remillard and Levine, 2008; Degenaar et al., 2012). It was first identified as an accreting NS LMXB with the X-ray burst on the 25$^{\text{th}}$ of June 2012. The burst on the 25$^{\text{th}}$ of June 2012 was further classified as a rare, energetic intermediate duration X-ray burst by Degenaar et al. (2013). IGR J17062-6143 is located at a distance of 7.3 ± 0.5 kpc (Keek et al., 2016).

3.4.2 Data description/lightcurve

On 26 June 2012, IGR J17062-6143 triggered Swift's BAT and slewed in 157 s to the source after which the XRT measurement started in WT mode. The measurement lasted around 950 s. In the lightcurve we see the decay of a thermonuclear X-ray burst. The BAT-trigger time is off from the start of the burst, which is approximately 150 s earlier.

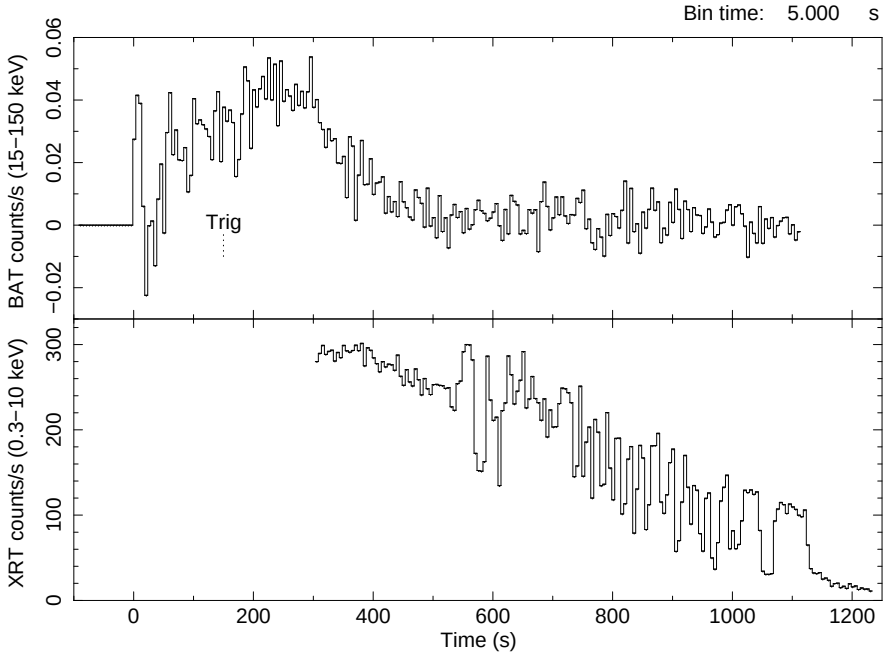

Figure 3.9: **IGR J17062-6143:** BAT and XRT lightcurves in 5s time bins. The start time (t=0) is set at 56103.944463 MJD The time at which the BAT triggered on this burst is displayed with a dotted line.

In the BAT lightcurve (see Fig. 3.9) are a lot of fluctuations at the start of the burst. These fluctuations are not significant because the errors are large in this section

of the curve. The errors are larger at that point because the source is off-axis in the beginning. Therefore, uncertainties are larger and become smaller as Swift slews towards the source. The first peak is a little more significant, as well as the dip just after the BAT-trigger time. The 'touchdown' point is around 300 s after the start of the burst, where the count rate reaches its maximum and after which the count rate decreases. The fluctuations start at around 540 s and go both up as down. This is 240 s after the BAT count rate starts decreasing, i.e. the touchdown. The dip at the end is likely a long dip, which is below the decay trend of the burst.

3.4.3 Hardness ratio

The hardness ratio declines as expected from a cooling blackbody (Fig. 3.10). The first fluctuation upward corresponds to the first dip in the hardness ratio. The final 2 longer dips are also visible as dips in the hardness ratio. The extreme peaks at the end of the 4.0-10/2.0-4.0 keV hardness ratio are an artefact of the very low count rate, and thus a large error, in the last 2 dips in these energy bands.

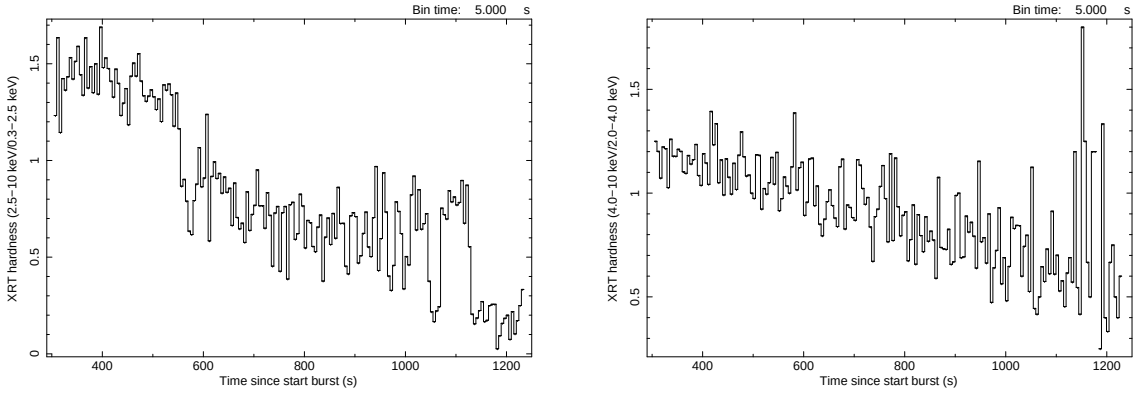

(a) (b)

Figure 3.10: IGR J17062-6143: Time profile of 2 hardness ratios.

3.4.4 Eddington limited burst

As seen in the burst from 4U 1850-087 (see § 3.2.4), this burst also shows a slow rise in count rate (see Fig. 3.9). Using the same argumentation, we argue that this burst is also Eddington limited.

3.4.5 Spectrum

The persistent emission as measured with MAXI from 56080 to 56110 MJD was below 0.02 counts cm^{-2} s^{-1} for both the 2.0-6.0 keV and 6.0-20.0 keV energy bands, with the exception of the days around the burst. The count rate of 0.02 is an upper limit and the average is around 0.01 counts cm^{-2} s^{-1}. Using the NASA `WebPIMMS` tool we

estimate the persistent flux (2.0-6.0 keV), which is $\sim 10^{-10}$ erg cm^{-2} s^{-1} for a powerlaw index of 2. The bolometric flux may be a factor $\sim$2 larger. Since we did not model the persistent spectrum we estimated the power law index. The persistent bolometric flux should therefore be taken with a large uncertainty of 50%. The persistent emission is however, much smaller than the burst emission at the start of the XRT data of 4.6×10^{-8} erg cm^{-2} s^{-1}. Therefore, we did not subtract the persistent emission in the spectra.

For the fluctuations spectrum we used the same model as Degenaar et al. (2013) did, except we did not fit the absorption lines and iron edges. In the fitted spectra one can clearly see the model is incorrect for the higher energies (see Fig. 3.11). Adding absorption lines and iron edges, as Degenaar et al. (2013) did, would improve this fit at higher energies. Interesting about the fluctuations spectrum is that an emission line around 1 keV is observed. There seems to be a much smaller drop in count rate between the up and down fluctuations around 1 keV. The emission line energy is in the Fe-L band. Degenaar et al. (2013) suggests that this emission line is caused by the irradiation of relatively cold gas. By dividing the full width at half maximum (FWHM) of the emission line by the line's energy, they derive a velocity of $\sim$0.16 c, where c is the speed of light. This velocity implies a radial distance of $\sim 8 \times 10^2$ km from the NS for a Keplerian orbit. Degenaar et al. (2013) also found absorption lines and edges at higher energies (> 7.5 keV) which we did not model. They conclude that the spectral features and the fluctuations (they use a time scale of 1-10 s) imply similar radial distances from the NS and are, therefore, likely caused by the same material and mechanism.

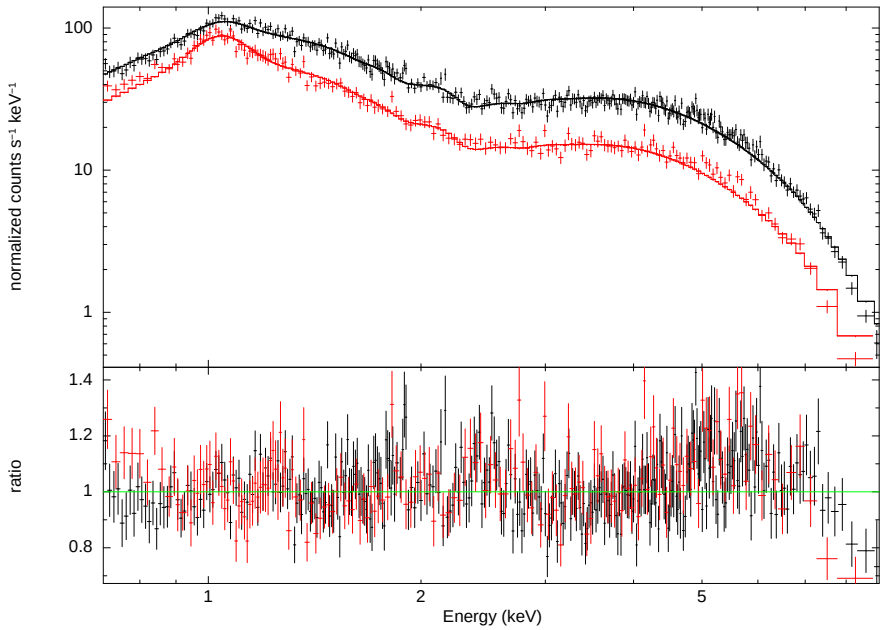

Figure 3.11: **IGR J17062-6143:** Spectrum of the fast fluctuations up (black) and down (red), modelled with two absorbed blackbodies and a Gaussian emission line from 230-650 s after XRT start.

Table 3.3: Spectral parameters for the spectra of the fluctuations up and down (see Fig. 3.11). The energies of the cooler blackbody and the energy and sigma of the Gaussian emission line are linked.

Model component	Parameter (unit)	Fluctuations up	Fluctuations down
TBABS	N_H ($\times 10^{22}$)	0.158 fix	0.158 fix
BBODYRAD	kT_{bb} (keV)	0.265 ± 0.003	0.265
BBODYRAD	norm ($\times 10^3$)	40.896 ± 2.592	27.417 ± 1.924
BBODYRAD2	kT_{bb} (keV)	1.7356 ± 0.0162	1.6274 ± 0.0227
BBODYRAD2	norm	161.805 ± 4.300	89.092 ± 3.674
GUASSIAN	E (keV)	1.0288 ± 0.0058	1.0288
GAUSSIAN	σ ($\times 10^{-2}$)	7.3795 ± 0.7805	7.3795
GAUSSIAN	norm ($\times 10^{-2}$)	8.4255 ± 1.0089	11.597 ± 1.0067
χ^2_{red}		Fitted same time	1.15168
Null hypothesis probability		Fitted same time	2.65×10^{-4}

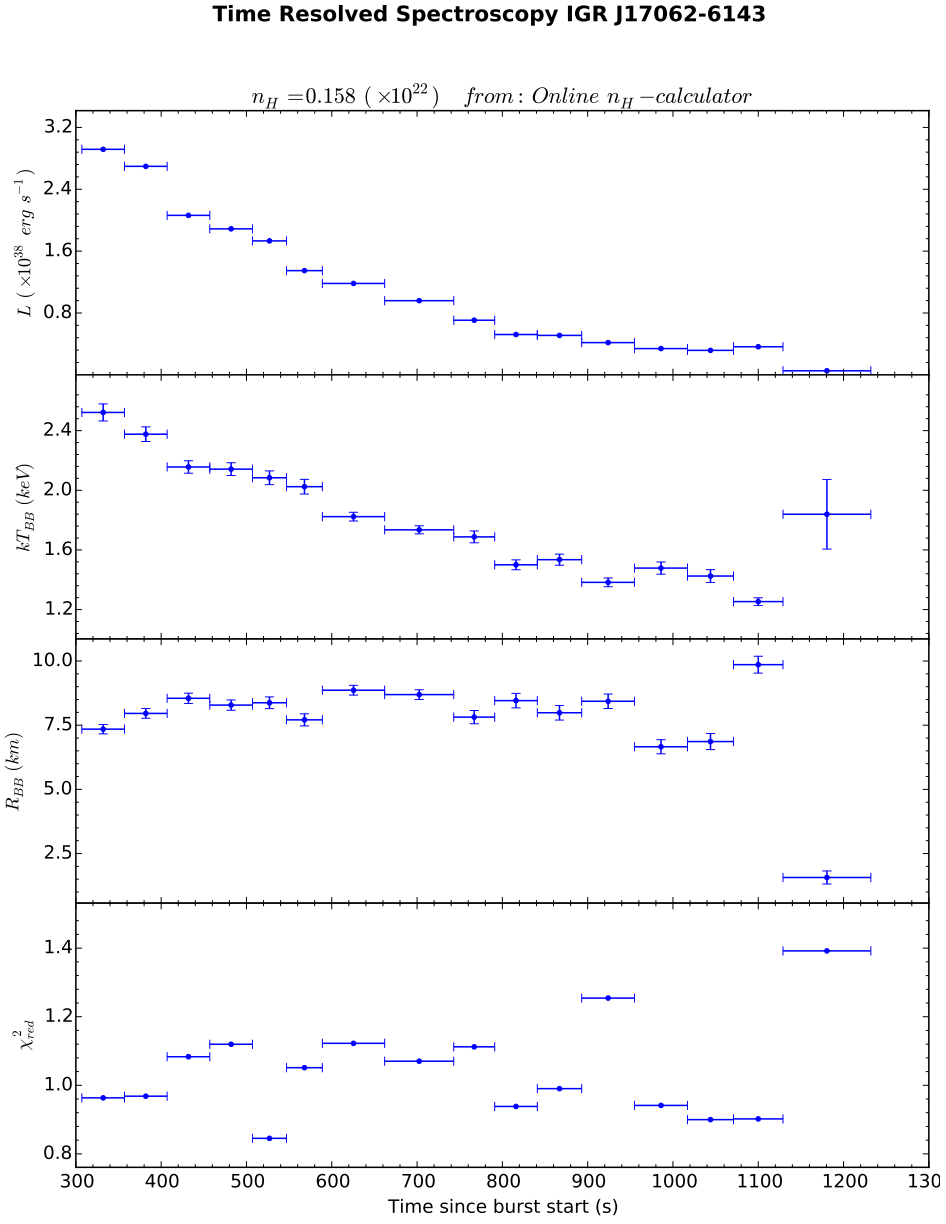

Figure 3.12: **IGR J17062-6143:** Time resolved spectroscopy for an assumed distance of 7.3 kpc.

3.5 SAX J1712.6-3739

3.5.1 General properties

SAX J1712.6-3739 was discovered in 1999 (in 't Zand et al., 1999), and is a persistent source. It is classified as a NS LMXB at a distance of 6-8 kpc (Cocchi et al., 2001). in't Zand et al. (2007) listed this source as a candidate UCXB, but Wiersema et al. (2009) argue that it is not a UCXB. Time resolved optical spectroscopy of this system would be able to reveal the binary period and therefore the UCXB nature. There are no papers published on bursts observed from this source with Swift. According to Yoon et al. (2011), SAX J1712.6-3739 is so far the only known X-ray binary to display a prominent H_α bow-shock nebula (Wiersema et al., 2009).

3.5.2 Data description/lightcurve

On 26 September 2011, SAX J1712.6-3739 triggered Swift's BAT and slewed in 121 seconds to the source after which the XRT measurement started in WT mode. The measurement lasted almost 60000 s but after 700 s there are only short bits of data with regular gaps of $\sim$ 6000 s (see Table 3.5, data coverage). In the lightcurve we see the decay of a thermonuclear X-ray burst.

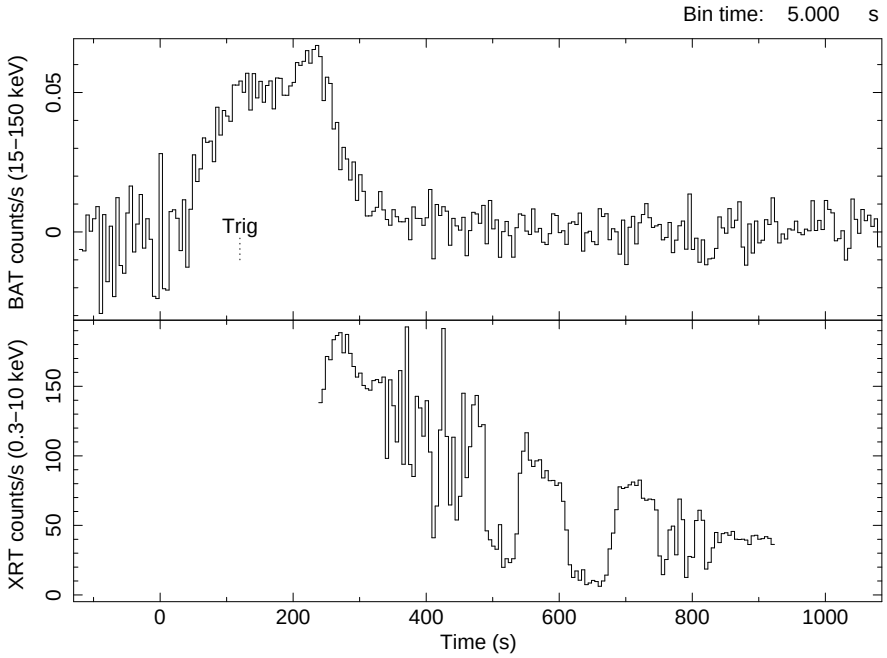

Figure 3.13: **SAX J1712.6-3739:** BAT and XRT lightcurves in 5s time bins. The start time (t=0) is set at 55830.839914 MJD The time at which the BAT triggered on this burst is displayed with a dotted line.

In the BAT data, a small precursor can be seen at which we set the burst start time (see Fig. 3.13). The end of the Eddington limited phase is around 240 s after

the start of the burst. The XRT lightcurve shows both fluctuations up as down. The faster fluctuations between $\sim$ 330 s and $\sim$ 480 s have both fluctuations up as down, whereas the longer dips only have fluctuations down. The fluctuations start $\sim$ 110 s after the touchdown of the photosphere. The beginning of the XRT data starts with a dip in the count rate. This dip could be the touchdown point, since it coincides with the peak in BAT count rate.

3.5.3 Hardness ratio

None of the dips are clearly visible in the hardness ratios. This burst has a much larger amount of hard photons than the other burst compared in this thesis. The hardness ratio between the 0.3-2.5 keV and 2.5-10 keV energy bands peaks at 6 and then decays from 4 to 3.

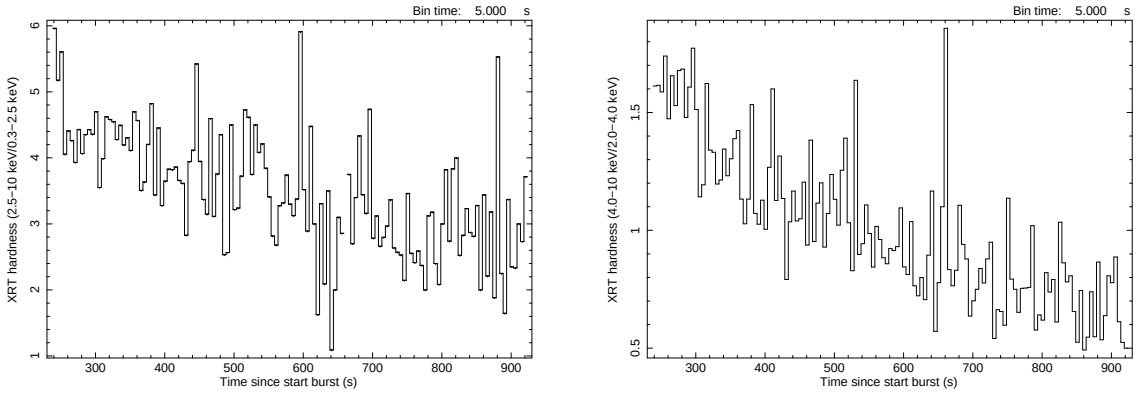

(a) (b)

Figure 3.14: SAX J1712.6-3739: Time profile of 2 hardness ratios.

3.5.4 Eddington limited burst

The BAT lightcurve also shows a slow rise in count rate (see Fig. 3.13). This is also seen in the bursts from 4U 1850-087 (see § 3.2.4) and IGR J17062-6143. Using the same argumentation, we argue that this burst is also Eddington limited.

3.5.5 Spectrum

For the time resolved spectroscopy (see Fig. 3.16) we fitted an absorbed blackbody. The χ^2_{red} values are also plotted. The spectra are not subtracted with the persistent flux of the source. The persistent flux measured with RXTE PCA on MJD 55828.100 was 32.17 counts s^{-1} $5PCU^{-1}$ (from Craig Markwardt[4]) translating to 3.217 mCrab (7.7208×10^{-11} erg cm^{-2} s^{-1}) which is insignificant compared to the burst emission.

[4] `https://asd.gsfc.nasa.gov/Craig.Markwardt/galscan/html/SAXJ1712.6-3739.html`

The maximum burst emission of the XRT data is 4.1×10^{-8} erg cm^{-2} s^{-1}. After the burst on MJD 55835.219 the persistent flux was 66.95 counts s^{-1} 5PCU^{-1}.

For the spectrum of the fluctuations (see Fig. 3.15) we selected the fluctuations between ∼340 and ∼480 s. The N_H value for this source is much higher than for the other three sources. Therefore, less can be said about the lower energies of this spectrum.

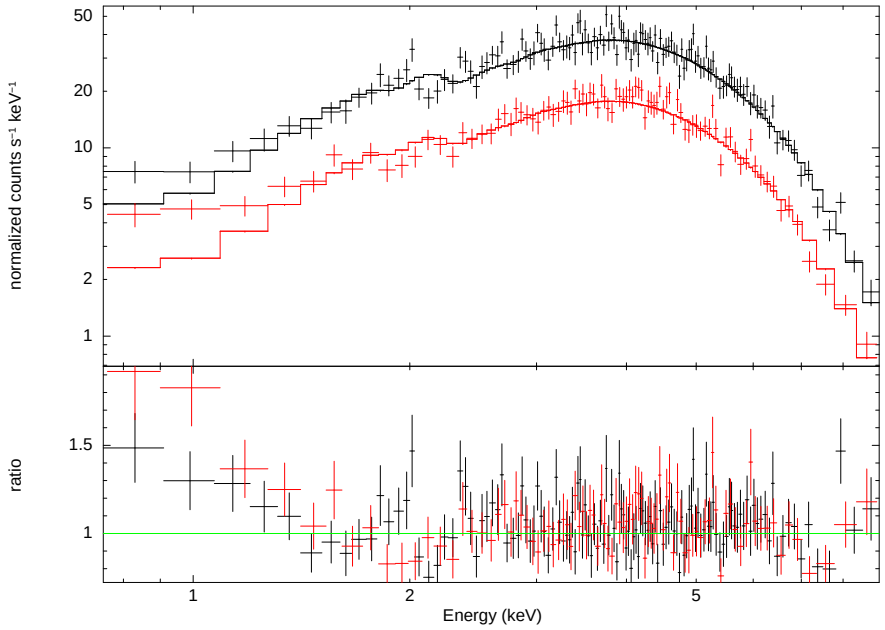

Figure 3.15: **SAX J1712.6-3739:** Spectrum of the fast fluctuations up (black) and down (red), modelled with an absorbed blackbody.

Table 3.4: Spectral parameters for the spectra of the fluctuations up and down. (Fig. 3.15)

Model component	Parameter (unit)	Fluctuations up	Fluctuations down
TBABS	N_H ($\times 10^{22}$)	1.34 fix	1.34 fix
BBODYRAD	kT_{bb} (keV)	1.9461 ± 0.0344	1.9305 ± 0.0395
BBODYRAD	norm	162.571 ± 7.420	78.440 ± 4.168
χ^2_{red}		Fitted same time	1.0505
Null hypothesis probability		Fitted same time	0.2011512

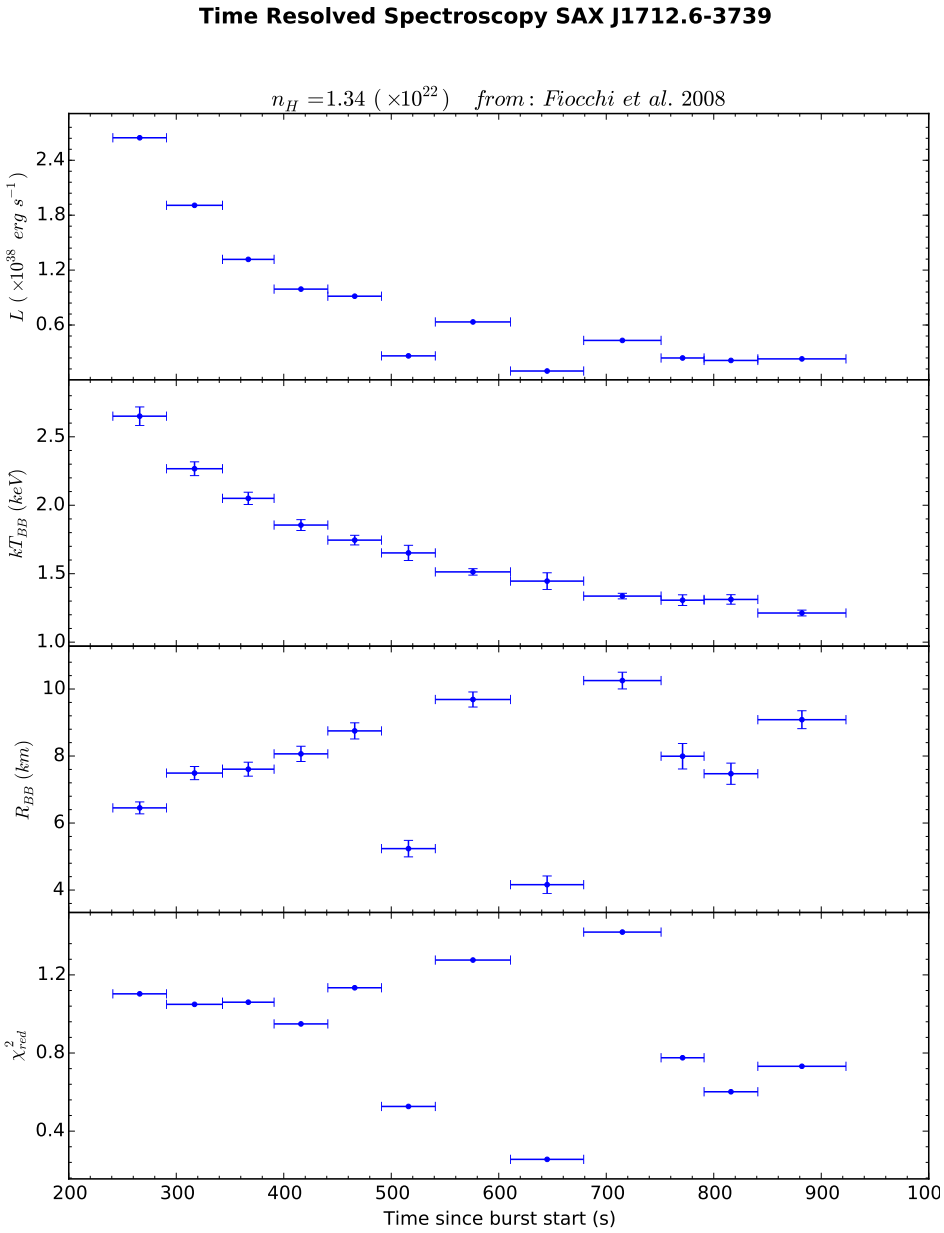

Figure 3.16: **SAX J1712.6-3739:** Time resolved spectroscopy for an assumed distance of 7 kpc.

3.6 Literature bursts

3.6.1 SLX 1735-269

SLX 1735-269 is a UCXB-candidate (in't Zand et al., 2007) which was first detected with the Spacelab 2 mission in 1985. Its LMXB and NS nature was confirmed in 1997 when a type-I X-ray burst was detected from the source. During observations of the Galactic Center region in 2003, INTEGRAL detected 6 type-I X-ray bursts of which one lasted over 1000 s (Molkov et al., 2005). This long burst (see Fig. 3.17) lasted over 2000 s and starts with a short precursor (2 s). 8 seconds after the precursor, the 'main' burst started. This burst has PRE and is Eddington limited. This burst also has superexpansion based on the fact that a precursor is seen. Molkov et al. (2005) estimated the distance to be between 6.0±1.2 kpc and 13±3 kpc, which was in agreement with an earlier estimate of 8.5 kpc. They conclude that the burst was most likely a result of the unstable burning of hydrogen and helium. This burst has a lot of fluctuations, both up and down in count rate. These fluctuations start before the touchdown (∼500 s).

3.6.2 A 1246-58

A 1246-58 is a UCXB-candidate (in't Zand et al., 2007) and was first identified as an NS-LMXB with the detection of an X-ray burst in 1997. in't Zand et al. (2008) investigated the UCXB nature of A 1246-58 further. 4 X-ray bursts were detected with the wide field camera (WFC) on BeppoSAX. All 4 bursts are Eddington limited, showing PRE. One of these 4 bursts can be seen in Fig. 3.18. in't Zand et al. (2008) derived a distance of 4.3 kpc in the case that the Eddington limit is that for a hydrogen-poor photosphere and corrected for gravitational redshift. An interesting feature of the lightcurve are the two dips between 80 and 150 s.

3.6.3 2S 0918-549

2S 0918-549 is a semi-confirmed UCXB (in't Zand et al., 2007) with a tentative orbital period of 17.4 min (Zhong and Wang, 2011). Three bursts were detected with the WFCs (in't Zand et al., 2005), one of which was much longer than the others, lasting over 2500 s. The first 1000 s of this long burst are displayed in Figure 3.19. The long burst showed a strong photospheric radius expansion. in't Zand et al. (2005) derive a distance of 5.4 kpc for a hydrogen-poor photosphere, if the peak bolometric flux equals the Eddington limit. There were two data drop outs: from 165 to 180 s and from 350 to 354 s. After ∼2 minutes a short period of strong fluctuations is observed. After these fluctuations a long dip starts quickly and then rises in ∼70 s back to the decay trend of the burst.

Five X-ray bursts were detected from this source with the proportional counter array (PCA) on the Rossi X-ray Timing Explorer (RXTE) (in't Zand et al., 2011). The last one (2008-02-08) is seven times longer than the next longest. This burst (see Fig. 3.20) has a precursor of 40 ms with the 'main' burst starting 1.2 s later. This

burst is Eddington limited and has PRE. The interesting feature of this burst is the strong fluctuations starting 122 s after burst onset and lasting 66 s.

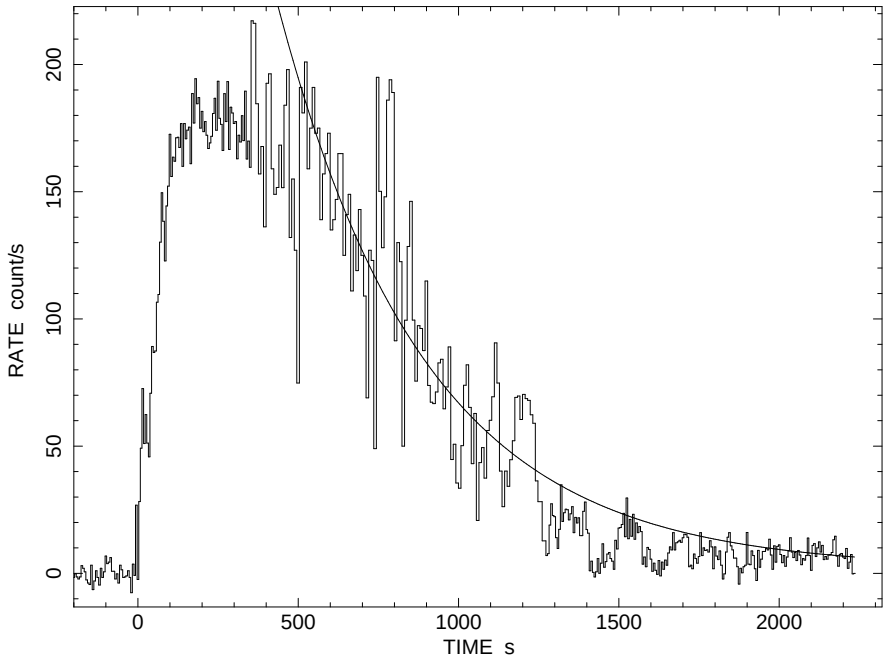

Figure 3.17: **SLX 1735-269:** JEM-X lightcurve. Starting on 52897.732801 MJD.

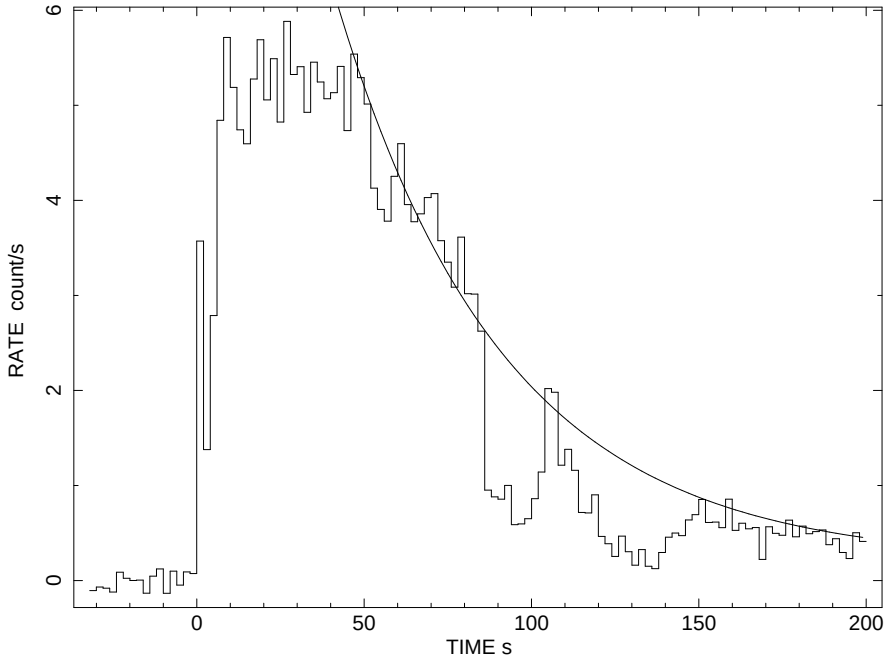

Figure 3.18: **A 1246-58:** WFC lightcurve. Starting on 50286.29006 MJD.

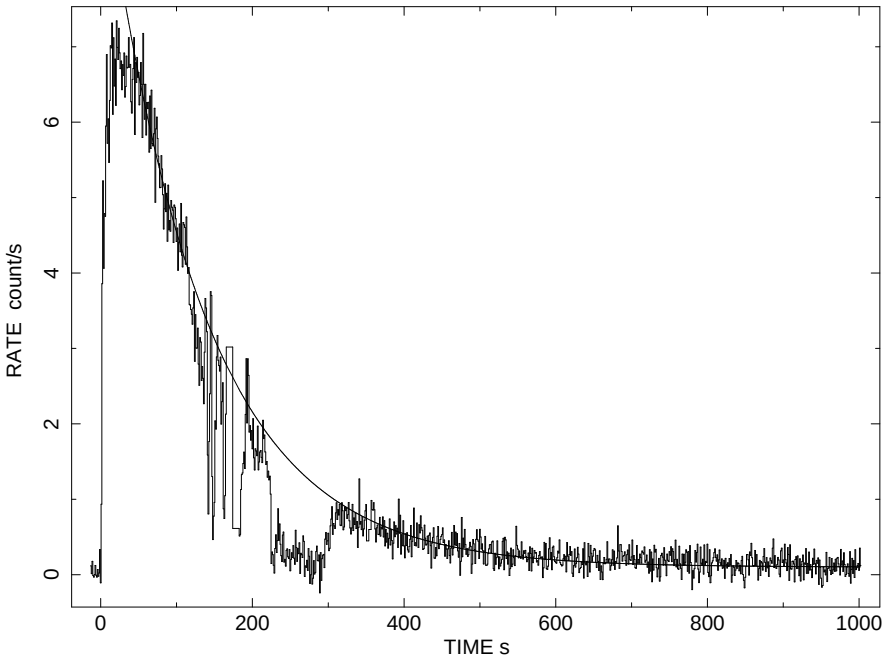

Figure 3.19: **2S 0918-549:** WFC lightcurve. Starting on 50357.885303 MJD.

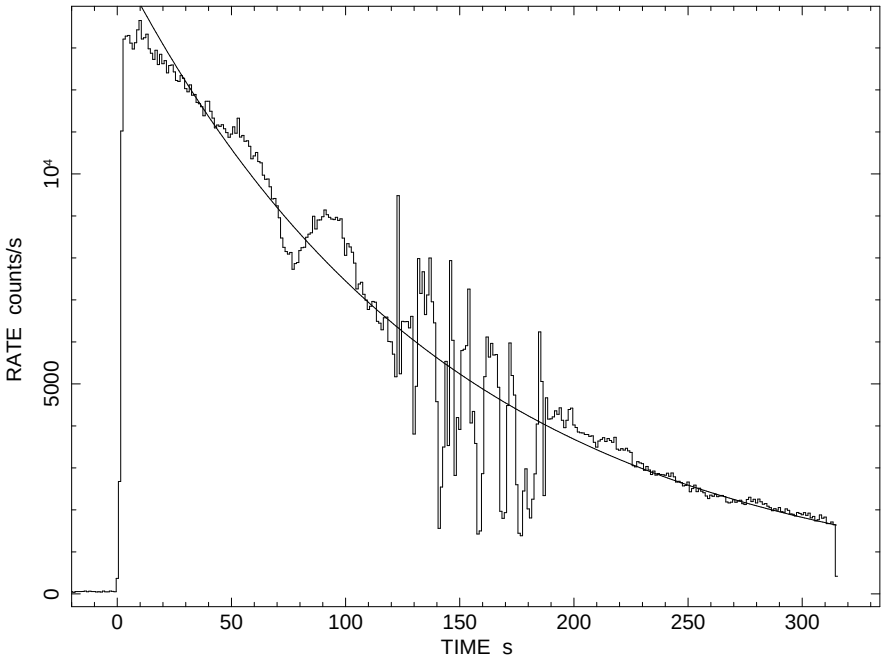

Figure 3.20: **2S 0918-549:** PCA lightcurve. Starting on 54504.126972 MJD.

3.7 Comparison between bursts

In this section we present three tables with information about the sources and bursts. In § 3.7.1 we explain how the values in the 3 tables are determined and in § 3.7.2 we summarize the most important findings from the tables.

3.7.1 Overview tables

Table 3.5 contains general information about the source including the type of binary, the hydrogen absorption column and the type of accretion with references. This table also includes information about the burst data.

Table 3.6 includes the e-folding decay times of the bursts. For this, the lightcurves were fitted with an exponential model with an added constant (`EXP+CONS`) in `FPLOT` and for the additional bursts from the literature we also added the e-folding decay times presented in their papers. For the bursts detected with Swift we determined the touchdown time by examining the peaks in the BAT lightcurves. Unless the touchdown time was reported in the reference of the literature burst, the touchdown time was estimated from the peak in the blackbody temperature (kT) plot. We also determined the timing properties of the fast fluctuations seen in the lightcurves (see Figs. 3.1; 3.5; 3.9; 3.13). The last column of this table presents how much the bolometric flux has dropped, as percentage of the peak flux, at the start of the fluctuations. For the calculation of the drop in bolometric flux we used the NASA HEASARC `WebPIMMS` tool. This tool allows us to simulate count rates and fluxes for different satellites. As input for the 4 Swift bursts we use the BAT peak count rate. The input energy range of the BAT is 15-150 keV and as output energy range we use 0.01-40 keV as bolometric flux for a blackbody. The tool then simulates the flux of a blackbody with a peak temperature. In the following list, we discuss some details about how the values in this column were derived.

- No fast fluctuations are present in the burst from 4U 1850-087.
- Bozzo et al. (2015) measured a peak blackbody temperature of ∼3.0 keV and an extrapolated bolometric flux (0.5-100 keV) of $(6.0 \pm 1.8) \times 10^{-8}$ erg cm^{-2} s^{-1}. When using the `WebPIMMS` tool we find 8.59×10^{-8} erg cm^{-2} s^{-1} (0.5-40 keV) for a blackbody of 3.0 keV. For the drop in bolometric flux calculation we used the peak flux value reported by Bozzo et al. (2015). Since there are fluctuations observed from the beginning of the XRT data, we used the bolometric flux of the first XRT data point. To calculate the drop in bolometric flux we used the luminosity just before the fluctuations derived by Bozzo et al. (2015): $\sim 1.1 \times 10^{38}$ erg s^{-1}, which translates to a bolometric flux of 1.77×10^{-8} erg cm^{-2} s^{-1}.
- Degenaar et al. (2013) reported a peak bolometric flux (0.01-100 keV) of 1.25×10^{-7} erg cm^{-2} s^{-1}. The bolometric flux (0.01-40 keV) measured just before the start of the fluctuations is taken from the time resolved spectroscopy at 500 s: 2.72×10^{-8} erg cm^{-2} s^{-1}.
- From 74 s before the trigger to 188 s after the trigger, the BAT data of the burst from SAX J1712.6-3739 was well fitted with a blackbody with a temperature of

2.7 keV (Palm, 2011). Using the `WebPIMMS` tool and a maximum BAT count rate of 0.065, we derive a bolometric flux (0.01-40 keV) of 1.17×10^{-7} erg cm^{-2} s^{-1}. Note that this is not the peak flux but a 262 s average. The drop in bolometric flux given in the table is therefore, most likely underestimated. From the time resolved spectroscopy we take the bolometric flux (0.01-40 keV) of the second interval: 2.99×10^{-8} erg cm^{-2} s^{-1}.

- For the burst from SLX 1735-269 the flux at the start of the fluctuations (7-10 keV and the bolometric luminosity) is the approximate pre-fluctuation maximum. Therefore, there is no drop in bolometric flux at the start of the fluctuations observed.
- The burst from A 1246-58 has a peak flux of $(9.5 \pm 0.5) \times 10^{-8}$ erg cm^{-2} s^{-1}, but no fluctuations are observed (in't Zand et al., 2008).
- The first burst from 2S 0918-549 (see Fig. 3.19) has a peak flux of 8.8×10^{-8} erg cm^{-2} s^{-1} (in't Zand et al., 2005). Although from Figure 4b: bolometric peak flux is $\sim1.1\times10^{-7}$ erg cm^{-2} s^{-1} and the flux just before the fluctuations is $\sim3.5\times10^{-8}$ erg cm^{-2} s^{-1}. For the calculation we used the peak flux from the figure.
- The second burst from 2S 0918-549 (see Fig. 3.20) has a peak flux of $\sim1.6\times10^{-7}$ erg cm^{-2} s^{-1} The bolometric flux just before the fluctuations is $\sim4\times10^{-8}$ erg cm^{-2} s^{-1}. These values are from Fig. 3: in't Zand et al. (2011).

In the last table (Table 3.7) we present timing properties of the eclipse-like features called 'dips'. When more than one eclipse-like feature is seen in the lightcurve, the dip duration column presents the average duration of the dips seen.

3.7.2 Important findings from the tables

The three tables are very useful to compare the 8 bursts. Below we note the most important findings.

- The e-folding decay times are all in the order of a few 100 s. The exception is the burst from A 1246-58, which has an e-folding decay time of ∼50 s. While this is at the lower end of the decay times, it is still much longer than the typical e-folding decay time of a 'normal' type-I X-ray burst. Hence, we can classify all 8 bursts as intermediate duration bursts.
- The fluctuations always start after the end of the Eddington-limited phase (i.e. after the touchdown). The burst from Swift J1734.5-3027 might be an exception because the fluctuations are already present at the start of the XRT data (see § 3.3.2).
- Two different phenomena are observed that have different time scales. Fluctuations and eclipse-like features.
- The fluctuations have a typical time scale in the order of ∼ 10 s.
- The eclipse-like features (or dips) have a typical duration of ∼ 60 s and most show a decay, similar to that of the burst, during the dip.
- The fluctuations with shorter time scales, if present, happen before the eclipse-like features with longer time scales.
- The drop in bolometric flux is comparable for all the bursts for which it could be

determined (except for the burst from SLX 1735-269), and is $\sim 75\%$.

Table 3.5: General properties and data coverage. All times are in seconds after the start of the burst, unless noted otherwise.

Object	Type	N_H ($cm^{-2} \times 10^{22}$)	P/T	Observation date (UTC) [YYYY-MM-DD HH:MM:SS]	Observation-ID	Instrument	Data coverage BAT(XRT) [s]
Case studies							
4U 1850-087	UCXB confirmed[1]	0.29[9]	P[1]	2014-03-10 21:01:40	00591237000	BAT+XRT	$-39(691) \Rightarrow (1444)$
Swift J1734.5-3027	LMXB[2]	0.84[2] [a]	T[2]	2013-09-01 09:09:42	00569022000	BAT+XRT	$-215(150) \Rightarrow (1691)$[b]
IGR J17062-6143	UCXB-cand[3]; LMXB[4]	0.158[3]	P[4]	2012-06-25 22:40:01	00525148000	BAT+XRT	$-89(307) \Rightarrow (1321)$
SAX J1712.6-3739	UCXB-cand[1],[5]	1.34[6]	P[1]	2011-09-26 20:09:28	00504101000	BAT+XRT	$-119(241) \Rightarrow (924)$[c]
Literature bursts					Satellite		
SLX 1735-269	UCXB-cand[1]	1.50[7]	P[1]	2003-09-15	INTEGRAL	JEM-X	$-1200 \Rightarrow 2235$
A 1246-58	UCXB-cand[1]	0.50[8]	P[1]	1996-07-22	BeppoSAX	WFC	$-31 \Rightarrow 199$
2S 0918-549	UCXB semi-confirmed[10]	0.35[9]	P[1]	1996-10-01	BeppoSAX	WFC	$-13 \Rightarrow 1002$
2S 0918-549	UCXB semi-confirmed[10]	0.35[9]	P[1]	2008-02-08	RXTE	PCA	$-768 \Rightarrow 315$

[a] Using $NH_{tot,mean}$ from `http://www.swift.ac.uk/analysis/nhtot/`: 1.03×10^{22}

[b] This data coverage is continuous. The rest of the XRT-WT data are short intervals: 5007-5017; 6510-6539; 7571-7583; 10772-10832; 12472-12505; 16550-16600 with count rates below 30c/s. PC data consists of 3 intervals: 5021-7546; 10836-13341; 16606-17346; with count rates below 9c/s.

[c] This data coverage is continuous. The rest of the XRT-WT data are short intervals: 5713-5808; 11556-11604; 17292-17296; 18999-19458(lot of mode switching to PC mode?); 23056-23128; 28820-28840; 34681-34684; 40387-40391; 46344-46360; 52324-52342; 58384-58400; with count rates below 30c/s. PC data consists of intervals: 5692-6257; 11492-12492; 13907-13962; 17182-18897; 23012-25517; 28727-30017; 34567-36017; 40277-40877; 46247-47597; 52227-52452; 58287-59102; with count rates below 9.5c/s.

References: [1]: in't Zand et al. (2007); [2]: Bozzo et al. (2015); [3]: Keek et al. (2016); [4]: Degenaar et al. (2013, 2017); [5]: Wiersema et al. (2009); [6]: Fiocchi et al. (2008); [7]: David et al. (1997); [8]: in't Zand et al. (2008); [9]: Juett et al. (2001); [10]: Zhong and Wang (2011)

Table 3.6: Burst properties and fast fluctuations. All times are in seconds after the start of the burst, unless noted otherwise. A dash means that there are no fast fluctuations seen.

Object	E-folding decay time [s]	Touchdown time [s]	Start FAST fluct. (after touchdown) [s]	Start FAST fluct. / Eddington phase duration	End time FAST fluctuations [s]	Time scale FAST fluct. [s]	Drop bol. flux until FAST fluct. [%]
Case studies							
4U 1850-087	1017 ± 29.8[a]	580	-	-	-	-	-
Swift J1734.5-3027	173.7 ± 3.0	80	Before start XRT	-	210	20	71
IGR J17062-6143	742.7 ± 30.95	300	540(240)	$\frac{540}{300} = 1.80$	1125	19	78
SAX J1712.6-3739	448.8 ± 29.35	240	330(110)	$\frac{330}{200} = 1.38$	480	11	74
Literature bursts							
SLX 1735-269	~ 460; [b]	420 [1]	380(-40)	$\frac{450}{420} = 1.07$	1230	49	0
A 1246-58	~ 50; 50-100[2]	55 [2]	-	-	-	-	-
2S 0918-549	~ 130; 117 ± 2[3]	85 [3]	135(50)	$\frac{135}{85} = 1.59$	195 (Data gap?)	9	68
2S 0918-549	~ 142; [c]	77 [4]	122(45)[13]	$\frac{122}{77} = 1.58$	188	6	75

[a] From ~ 20 s to ~ 300 s the lightcurve is flattened. If the exponential function is fitted to the lightcurve after this flat phase, the e-folding time decreases significantly to 130.37 ± 31.35 s. More information in § 3.2.

[b] 250 ± 20 (2-7 keV)[1]

[c] 149.3 ± 3.1 (< 4 keV) & 113.4 ± 1.2 (> 4 keV); see [4]

References: [1]: Molkov et al. (2005); [2]: in't Zand et al. (2008); [3]: in't Zand et al. (2005); [4]: in't Zand et al. (2011);

Table 3.7: Longer dip properties. All times are in seconds after the start of the burst, unless noted otherwise. A dash means that there are no dips seen. When more dips are seen, an average duration of the dips is given.

Object	Start dips [s]	End dips [s]	Ingress & egress time [s]	Dip duration [s]	Decay during dip?
Case studies					
4U 1850-087	1020 or 1240	Beyond data or 1270	1 & 2	30	Yes
Swift J1734.5-3027	210	320	3 & 3	38	No, Stepping
IGR J17062-6143	1125	Beyond data coverage?	3 & 3	≥ 107	Yes
SAX J1712.6-3739	480	840	8 & 3 (or 9)	60	Yes, a little
Literature bursts					
SLX 1735-269	1230	1652	5 & 10	80	No
A 1246-58	85	150	2 & 4; 4 & 8	30	Yes
2S 0918-549	220	310	2 & 70	90	Yes
2S 0918-549	-	-	-	-	-

Chapter 4

Discussion

This chapter summarises the findings, discusses the similarities of the sources and bursts, and interprets the findings.

4.1 Findings

Of the 7 sources discussed in § 3, 6 are (candidate-) UCXBs, which implies a small orbit. Orbital periods for UCXBs range from ∼11 min to 1.5 h. Therefore, the binaries have a small accretion disk and almost certainly a hydrogen-poor donor star (Nelson et al., 1986; Savonije et al., 1986). Not much is known about the orbital properties of Swift J1734.5-3027.

The sources 4U 1850-087, 2S 0918-549, A 1246-58, SAX J1712.6-3739 and SLX 1735-269 are not known to be dippers and/or eclipsers (in't Zand et al., 2007). Dips are due to a bulge of the accretion disk, where the accretion stream impacts the accretion disk. Eclipses are due to the donor star. Both features obscure the line of sight to the inner X-ray bright part of the disk. Dips and/or eclipses from the sources Swift J1734.5-3027 and IGR J17062-6143 have also not been seen, although one should note that they have not been observed much yet. This indicates that the sources are all viewed from a relatively small inclination angle (see Fig. 4.1).

The bursts are all intermediate duration bursts, lasting longer than normal Type-I X-ray bursts (tens of seconds) but shorter than 'superbursts' (several hours). One is tempted to attribute the fluctuations that we see to a selection effect because it is, of course, more likely to see fluctuations in longer bursts than in shorter ones. However, short bursts have been seen ∼100 times as many as intermediate duration bursts, which counteracts this selection effect.

The bursts all have photospheric radius expansion and SLX 1735-269 (Molkov et al., 2005), 2S 0918-549 (in't Zand et al., 2011), A 1246-58 (in't Zand et al., 2008) show superexpansion, the latter two reaching an emission radius of over 1000 km. The first burst from 2S 0918-549 (in't Zand et al., 2005) does not have superexpansion unless the precursor last shorter than ∼0.1 s like in the second burst, when it would not be detectable. For the 4 bursts detected with Swift, no XRT data are available for the first 100 s. Therefore, it is impossible to check whether superexpansion happened.

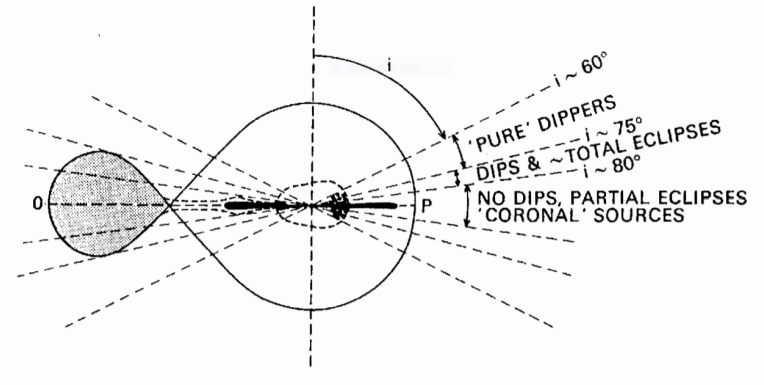

Figure 4.1: Dip and eclipse properties for different inclination angles between the disk axis and the line of sight. In the figure the accretion disk is viewed from the side. (From Frank et al., 2002)

Degenaar et al. (2013) suggest that it is plausible that superexpansion happened in the burst from IGR J17062-6143.

Comparing the spectra from 4U 1850-087 (Fig. 3.3) and IGR J17062-6143 (Fig. 3.11), we see that both have an interesting feature just above 1 keV. Although we are looking at two different parts of the burst (at the dip for 4U 1850-087 and at the fluctuations for IGR J17062-6143), they have similar features. Logically, the count rate is lower for the downward fluctuations than the count rate for the upward fluctuations, but around 1 keV the difference in count rate is much smaller. In the case of 4U 1850-087 the count rate is approximately equal around 1 keV for both the dip (∼30 s) and the times around the dip (30 s before until the dip start and from the end of the dip to 30 s after the dip). A small peak in the downward fluctuations of Swift J1734.5-3027 (Fig. 3.8) is also visible around ∼1.4 keV. The model in that spectrum is also underestimated in the 1 keV area as is the case with 4U 1850-087 and IGR J17062-6143. The 1 keV emission feature is present in those 3 bursts, although most prominent in the burst from IGR J17062-6143. SAX J1712.6-3739 has a N_H-value which is much higher than for the other three bursts which makes it difficult to detect any feature in the spectrum below 2 keV (see Fig. 3.15).

The burst from SAX J1734.5-3027 differs from the other bursts in that it has a much harder spectrum (for the spectrum, see Fig. 3.15). This is best seen in the hardness ratio (see Fig. 3.14, a) which peaks at a ratio of 6, then drops to 4 and decays slowly to a ratio of 3. The other bursts start at maximum at a ratio of 3 and then decay to a ratio of 1 or lower.

Looking further at the variability in the bursts, we can distinguish two different types of variability: fast fluctuations both up and down and eclipse-like features only down. The fluctuations have a typical time scale of ∼10 s (see Table 3.6) and an amplitude of ∼70% ($\frac{max-min}{2}$ in percentage of the count rate at the centre of the fluctuation). In the eclipse-like features the flux only goes down by ∼90% but not up. In most cases the burst decay remains visible at a lower flux in most cases (see Table 3.7). This is not the case for the burst from Swift J1734.5-3027 where halfway

the two dips the flux suddenly rises to a level between the first part of the dip and the out-of-dip decay (see Fig. 3.5). 5 of the 8 bursts discussed here have both types of variabilities, 2 only have eclipse-like features and 1 only has the fluctuation feature (the touchdown is not counted as an eclipse-like feature in Fig. 3.20).

The variability always occurs after the PRE-phase (i.e. after the touchdown) except for SLX 1735-269 where the variability seems to occur ∼40 s before the touchdown point. The fluctuations start at $1.5^{+0.3}_{-0.4}$ times the PRE duration for the 5 bursts for which this ratio could be determined. The fluctuations and dips are visible in the hardness ratio of 2.5-10/0.3-2.5 keV for all the burst, except for the one from SAX J1712.6-3739, but are never seen in the hardness ratio of 4.0-10/2.0-4.0 keV. As described above the fluctuations are not seen in both the hardness ratios of SAX J1712.6-3739. This suggests that the fluctuations are not achromatic as earlier suggested by in't Zand et al. (2011).

4.2 Interpretation

4.2.1 Origin of fluctuations

The fluctuations go several tens of percents above and below the decay trend of the burst. One idea for the upward fluctuations in flux is that they could be due to small thermonuclear flashes happening during the decay phase of the burst. However, the fact that the upward fluctuations are always followed by downward fluctuations is then unexplained. Furthermore, we do not observe changes in the spectrum as would be expected from a surge in heating.

The fluctuations look like dips where the inner accretion disk is obscured from the line of sight by irregularities of the outer disk, or eclipses where the donor blocks the view of the NS. What differentiates the fluctuations from dips and eclipses is the addition of upward fluctuations. Since these fluctuations are not observed when the source is not bursting, this origin of the fluctuations is less clear cut. A strong suspicion relates to the superexpansive character because these fluctuations have never been seen in bursts which clearly do not have PRE but last sometimes just as long.

Continuing on the idea of the dip/eclipse-like character, there must be some irregularity around the NS which covers the emission area occasionally. One can image that superexpansion, where a whole shell is blown off the NS's surface reaching far into the accretion disk, can disrupt the accretion disk as a whole as a result of the passing shell/wind and the strong radiation pressure. As a consequence, many irregularities should be created in the disk. However, strong fluctuations are seen making it more probable that only one or two larger irregularities are causing the fluctuations instead of many. Such large irregularities could be a large part of the accretion disk wobbling up and down.

When this irregularity is located at the inner accretion disk, it moves fast around the NS because the Kepler period is shorter, causing fast fluctuations. When the irregularity is located somewhat further out in the accretion disk, it causes the longer eclipse-like features. Fluctuations going up could subsequently be explained by the

fact that, when the irregularity is on the other side of the NS but visible, photons are scattered back into the line of sight. In the case of an irregularity located close to the NS: a small irregularity can cause a large reflection component since the angle subtended, as seen from the NS is large. The same irregularity located further away from the NS causes a much smaller reflection-component, since this angle is smaller.

In the bursts that have both types of variabilities, two characteristic time scales are observed. The ratios of the time scales (eclipse/fluctuation) are: 1.9; $\geq$5.6; 5.5; 1.6 and 10 for Swift J1734.5-3027, IGR J17062-6143, SAX J1712.6-3739, SLX 1735-269 and 2S 0918-549 respectively. There seems to be no relation between the eclipse and fluctuation time scales. The time scales of the fast fluctuations (see Table 3.6) imply a distance to the neutron star of approximately 1.2; 1.2; 0.8; 2.2; 0.7/0.6 $\times 10^4$ km for Swift J1734.5-3027, IGR J17062-6143, SAX J1712.6-3739, SLX 1735-269 and 2S 0918-549 (9 and 6 s fluctuations) respectively, for Keplerian orbits (a NS mass of 1.4 $M_\odot$ is assumed). When looking at the fluctuations of the burst from IGR J17062-6143 in a higher time resolution (0.5 s), there appear to be fluctuations on that time scale. This would imply a radial distance of $\sim 10^3$ km from the NS.

It remains difficult to explain the two distinct time scales and why not a multitude of time scales are observed. An explanation may be that these bursts all roughly have the same power and that therefore, the irregularities are located at roughly the same distance from the NS. The time scale of the fluctuations in the SLX 1735-269 burst is $\sim$2 times longer than the other bursts. For Keplerian orbits the distance scales as $P^{2/3}$. A time scale $\sim$2 times larger implies a distance of $\sim$1.6 times further from the NS. This is probably the result of the longer Eddington limited phase, which is after the burst from 4U 1850-087 the longest (see Table 3.6).

4.2.2 Accretion disk disruption

What could be the origin of these irregularities in the accretion disk? Two possible mechanisms for creating irregularities, which are most probable for bursts with super-expansion according to in't Zand et al. (2011), are disruption by an expanding shell and disruption by radiation pressure.

The shell is geometrically thin (at maximum 1% of the ignition column depth) and optically thick. This shell is blown off the NS surface at a velocity of a tenth of the speed of light. This shell can have enough momentum to sweep the inner 100 km of the accretion disk and may be able to disrupt the disk up to a distance of approximately 3000 km (in't Zand et al., 2011) when the shell moves over the accretion disks surface. This is due to the RAM pressure that the shell carries. The shell has passed the accretion disk very quickly (within seconds), after which a strong wind due to radiation pressure takes over. Because the shell has likely cleared the inner accretion disk, the effect of radiation pressure extends radially further. This extended radiation pressure is probably preventing the disk from falling back during near-Eddington fluxes. Since the shell has cleared the inner disk, it is likely that the inner edge of the disk is puffed up. This increases the effect of radiation pressure because the angle subtended by the accretion disk as seen from the NS is increased. This wind also skims over the

surface of the accretion disk. This could sweep up local structures on the accretion disk. This effect is increased by the shell that has past the disk, probably creating a rough surface of the disk. When the wind skims over this rough surface the flow becomes more turbulent puffing the disk up even more. Together these mechanisms disturb the accretion disk and create irregularities causing the observed fluctuations. However, the typical scale may be too small to explain that we see strong fluctuations.

Imagine a flag waving in the wind. When the wind flows past the flag this causes the flag to flutter, with growing amplitude as the distance to the end of the flag decreases. This can be compared to the accretion disk in the sense that a small (in amplitude) structure can cause a fluctuation in the lightcurve and when the structure is located further from the NS, the size of the structure has to be much larger to achieve a similar fluctuation. Just like a particle in the fabric of a flag moves up and down, a structure created on the accretion disk could possible also move up and down (z-direction) the accretion disk. Equivalent to the wind blowing past the flag, a wind consisting of photons and particles due to radiation pressure blows across the accretion disk. A strong wind flowing past the flag creates fluctuations with small amplitudes in the flag which have a short wavelength. When the strength of the wind decreases, the flag is allowed to have larger fluctuations and also larger wavelengths. When we apply this analogy to the observations we can explain that, at first only short fluctuations are seen and later large dips with a longer time scale. At the start of the burst the wind is relatively strong and during the decay of the burst, the radiation pressure of this wind decreases. As a consequence of this decreasing wind, the fluctuations become larger in amplitude and longer in wavelength. However, this analogy does not explain the two different time scales of the variabilities that are observed.

4.2.3 Delay of fluctuations

The fact that the fluctuations start at $1.5^{+0.3}_{-0.4}$ times the PRE duration is puzzling. It is interesting that the fluctuations do not start right after the PRE phase. At the end of the PRE phase, the photosphere is back at the NS surface and there is no more wind from the radiation pressure. When the fluctuations start, the PRE phase has ended for around a minute or more. There may be some viscous process which delays the fluctuations and prevents the irregularities from floating in the line of sight directly. The viscous (or radial drift) time scale is defined as:

$$t_{visc} \sim R^2/\nu \tag{4.1}$$

where ν is the viscosity and R the radial distance (Eq. 5.9 in Frank et al., 1992). This gives an estimate of the time scale for a disc annulus (i.e. a ring in the accretion disk) to move a radial distance R. For a gas-pressure dominated accretion disk t_{visc} becomes (in't Zand et al., 2011; Ballantyne and Everett, 2005):

$$t_{visc} = 4\alpha_{0.1}^{-4/5} M_{1.4}^{8/5} \dot{M}_{16}^{-2/5} (R/R_g)^{7/5} J(R)^{-2/5} \text{ s} \tag{4.2}$$

with α the disk viscosity parameter (Shakura and Sunyaev, 1973) in units of 0.1, $M_{1.4}$ the NS mass in units of 1.4 $M_\odot$, $\dot{M}_{16}^{-2/5}$ the accretion rate in units of 10^{16} g s^{-1},

$R_g = GM/c^2$ and $J(R) = 1 - \sqrt{6R_g/R}$. In general for UCXBs the values of the parameters in Eq. 4.2 are the same order as the units they are in. The accretion rate is approximately 1% of the Eddington rate (which is $\sim 10^{18}$ g s^{-1}). Therefore t_{visc} depends only on the radial term. $R_g \simeq 3$ km $M_\odot{}^{-1}$ and we take $R = 100$ km, then the viscous time scale is ∼85 s. This is in the same order as the delay time of the fluctuations. The radiation pressure may increase this time because it may prevent matter from moving towards the NS or slow it down if this pressure is strong enough (see § 4.2.1).

For the two bursts of 2S 0918-549 the ratio between the start of the fluctuations and the PRE duration is almost exactly the same (see Table 3.6), which may imply that this ratio is dependent on the binary and not specifically on the properties of the burst (the second burst does not have eclipse-like features). Future bursts from this source with PRE and fluctuations could confirm this.

We can also attempt to explain the delay of the fluctuations with the analogy of the flag. The shell has swept the inner 100 km of the accretion disk. It is probably the resettling of the accretion disk within this first 100 km that is causing the variabilities. At the beginning of the burst the wind due to radiation pressure is very strong. This prevents matter of the accretion disk from flowing towards the NS and delaying the start of the fluctuations. When the radiation pressure decreases below the Eddington-limit, matter will flow towards the NS. Radiation can still prevent fluctuations similar to a flag. A strong wind causes the flag to be flat and have no fluctuations at all, because any deviation from the plane of the flag is directly pushed back by the pressure of the wind. The radiation pressure may still be strong enough to eliminate fluctuations after the PRE phase. This could explain the delay of fluctuations observed.

In order to verify the explanations, for the fluctuations and eclipse-like features seen in these 8 bursts, given in this discussion quantitative work needs to be done. This future work is most needed in the modelling of the accretion disk and how it responds to bursts, like the 8 bursts in this thesis. Constraints for this modelling are the superexpansive character of these bursts but also the fact that all 8 bursts discussed here are UCXBs or UXCB-candidates. Furthermore, there is a lack of hydrogen in the composition of the accretion disk and the burst fuel as a result of the ultracompact nature of these binaries (see § 1.2). The phenomena discussed here also provide interesting possibilities to study the accretion disk and its properties. Whereas normally the properties of the accretion disk are dictated by the donor star, this is now done by the accretor (i.e. the NS).

Chapter 5

Conclusion

We found 4 bursts with eclipse-like features and strong fluctuations during their decay, in Swift data. The 4 bursts are discussed in detail and are from: 4U 1850-087, Swift J1734.5-3027, IGR J17062-6143 and SAX J1712.6-3739. 4 additional bursts from the literature which show similar features were also considered but not studied in such detail. We provide a table with information about all 8 bursts, their variabilities and general properties of the source.

We find that the typical time scale of the fluctuations is in the order of $\sim$10 s and go $\sim$70% above and below the burst decay trend. The variabilities (fluctuations and eclipse-like features) almost always occur after the PRE-phase. The one exception is tentative because of lower data quality (see § 3.3.2).

The fluctuations show similar spectral characteristics such as an emission line around $\sim$1 keV. The spectrum does not change, except in total emission, between upward and downward fluctuations. The emission from this line is relatively stronger for the downward fluctuations.

As previously suggested by in't Zand et al. (2011), the fluctuations are possibly due to a disturbed accretion disk, which is likely caused by a combination of an expanding shell and a near-Eddington flux. These causes provide an explanation for the variabilities seen in these 8 bursts. The validity of this suggestion needs to be verified through modelling the interaction of shells, winds and radiation pressure and the accretion disk with as constraints the superexpansive character of the bursts, the ultracompact nature of the binaries and the lack of hydrogen in the composition of the burst fuel and the accretion disk.

References

Antoniadis, J., Freire, P. C. C., Wex, N., Tauris, T. M., Lynch, R. S., van Kerkwijk, M. H., Kramer, M., Bassa, C., Dhillon, V. S., Driebe, T., Hessels, J. W. T., Kaspi, V. M., Kondratiev, V. I., Langer, N., Marsh, T. R., McLaughlin, M. A., Pennucci, T. T., Ransom, S. M., Stairs, I. H., van Leeuwen, J., Verbiest, J. P. W., and Whelan, D. G.: 2013, *Science* **340**, 448

Ballantyne, D. R. and Everett, J. E.: 2005, *Astrophysical Journal* **626**, 364

Barthelmy, S. D., Barbier, L. M., Cummings, J. R., Fenimore, E. E., Gehrels, N., Hullinger, D., Krimm, H. A., Markwardt, C. B., Palmer, D. M., Parsons, A., Sato, G., Suzuki, M., Takahashi, T., Tashiro, M., and Tueller, J.: 2005, *Space Science Reviews* **120**, 143

Bevington, P. R. and Robinson, D. K.: 1992, *Data reduction and error analysis for the physical sciences*

Bozzo, E., Romano, P., Falanga, M., Ferrigno, C., Papitto, A., and Krimm, H. A.: 2015, *A&A* **579**, A56

Burrows, D. N., Hill, J. E., Nousek, J. A., Kennea, J. A., Wells, A., Osborne, J. P., Abbey, A. F., Beardmore, A., Mukerjee, K., Short, A. D. T., Chincarini, G., Campana, S., Citterio, O., Moretti, A., Pagani, C., Tagliaferri, G., Giommi, P., Capalbi, M., Tamburelli, F., Angelini, L., Cusumano, G., Bräuninger, H. W., Burkert, W., and Hartner, G. D.: 2005, *Space Science Reviews* **120**, 165

Cavecchi, Y.: 2013, *Ph.D. thesis*, University of Amsterdam; University of Leiden

Churazov, E., Sunyaev, R., Revnivtsev, M., Sazonov, S., Molkov, S., Grebenev, S., Winkler, C., Parmar, A., Bazzano, A., Falanga, M., Gros, A., Lebrun, F., Natalucci, L., Ubertini, P., Roques, J.-P., Bouchet, L., Jourdain, E., Knödlseder, J., Diehl, R., Budtz-Jorgensen, C., Brandt, S., Lund, N., Westergaard, N. J., Neronov, A., Türler, M., Chernyakova, M., Walter, R., Produit, N., Mowlavi, N., Mas-Hesse, J. M., Domingo, A., Gehrels, N., Kuulkers, E., Kretschmar, P., and Schmidt, M.: 2007, *A&A* **467**, 529

Cocchi, M., Bazzano, A., Natalucci, L., Ubertini, P., Heise, J., Kuulkers, E., Cornelisse, R., and in't Zand, J. J. M.: 2001, *A&A* **378**, L37

David, P., Goldwurm, A., Murakami, T., Paul, J., Laurent, P., and Goldoni, P.: 1997, *A&A* **322**, 229

Degenaar, N., Altamirano, D., and Wijnands, R.: 2012, *The Astronomer's Telegram* 4219

Degenaar, N., Miller, J. M., Wijnands, R., Altamirano, D., and Fabian, A. C.: 2013, *Astrophysical Journal, Letters* **767**, L37

Degenaar, N., Pinto, C., Miller, J. M., Wijnands, R., Altamirano, D., Paerels, F., Fabian, A. C., and Chakrabarty, D.: 2017, *Monthly Notices of the RAS* **464**, 398

Falanga, M., Chenevez, J., Cumming, A., Kuulkers, E., Trap, G., and Goldwurm, A.: 2008, *A&A* **484**, 43

Fiocchi, M., Bazzano, A., Ubertini, P., Bird, A. J., Natalucci, L., and Sguera, V.: 2008, *A&A*

492, 557
Frank, J., King, A., and Raine, D.: 1992, *Accretion Power in Astrophysics*, No. 20 in Cambridge astrophysics series, Cambridge University Press, 2nd edition
Frank, J., King, A., and Raine, D. J.: 2002, *Accretion Power in Astrophysics: Third Edition*
Harris, W. E.: 1996, *Astronomical Journal* **112**, 1487
Hawking, S. W. and Israel, W.: 1989, *Three Hundred Years of Gravitation*
Homer, L., Charles, P. A., Naylor, T., van Paradijs, J., Auriere, M., and Koch-Miramond, L.: 1996, *Monthly Notices of the RAS* **282**, L37
in 't Zand, J., Heise, J., Bazzano, A., Cocchi, M., and Smith, M. J. S.: 1999, *IAU Cirulars* 7243
in 't Zand, J. J. M. and Weinberg, N. N.: 2010, *A&A* **520**, A81
in't Zand, J. J. M., Bassa, C. G., Jonker, P. G., Keek, L., Verbunt, F., Méndez, M., and Markwardt, C. B.: 2008, *A&A* **485**, 183
in't Zand, J. J. M., Cumming, A., van der Sluys, M. V., Verbunt, F., and Pols, O. R.: 2005, *A&A* **441**, 675
in't Zand, J. J. M., Galloway, D. K., and Ballantyne, D. R.: 2011, *A&A* **525**, A111
in't Zand, J. J. M., Homan, J., Keek, L., and Palmer, D. M.: 2012, *A&A* **547**, A47
in't Zand, J. J. M., Jonker, P. G., and Markwardt, C. B.: 2007, *A&A* **465**, 953
Juett, A. M., Psaltis, D., and Chakrabarty, D.: 2001, *Astrophysical Journal, Letters* **560**, L59
Kass, R. E. and Raftery, A. E.: 1995, *Journal of the American Statistical Association* **90(430)**, 773
Keek, L., Iwakiri, W., Serino, M., Ballantyne, D. R., in 't Zand, J. J. M., and Strohmayer, T. E.: 2016, *ArXiv e-prints*
Kumar, P. and Zhang, B.: 2015, *Physics Reports* **561**, 1
Kutschera, M.: 1998, *Acta Physica Polonica B* **29**, 25
Kuulkers, E., den Hartog, P. R., in't Zand, J. J. M., Verbunt, F. W. M., Harris, W. E., and Cocchi, M.: 2003, *A&A* **399**, 663
Kuulkers, E., in't Zand, J. J. M., van Kerkwijk, M. H., Cornelisse, R., Smith, D. A., Heise, J., Bazzano, A., Cocchi, M., Natalucci, L., and Ubertini, P.: 2002, *A&A* **382**, 503
Lattimer, J. M. and Prakash, M.: 2004, *Science* **304**, 536
Lewin, W. H. G. and Joss, P. C.: 1981, *Space Science Reviews* **28**, 3
Lewin, W. H. G., van Paradijs, J., and Taam, R. E.: 1993, *Space Science Reviews* **62**, 223
Mazzali, P. A., Röpke, F. K., Benetti, S., and Hillebrandt, W.: 2007, *Science* **315**, 825
Molkov, S., Revnivtsev, M., Lutovinov, A., and Sunyaev, R.: 2005, *A&A* **434**, 1069
Nelemans, G., Wood, M., Groot, P., Anderson, S., Belczynski, K., Benacquista, M., Charles, P., Cumming, A., Deloye, C., Jonker, P., Kalogera, V., Knigge, C., Marsh, T., Motl, P., Napiwotzki, R., O'Brien, K., Phinney, E. S., Ramsay, G., Shahbaz, T., Solheim, J.-E., Steeghs, D., van der Sluys, M., Verbunt, F., Warner, B., Werner, K., Wu, K., and Yungelson, L. R.: 2009, in *astro2010: The Astronomy and Astrophysics Decadal Survey*, Vol. 2010 of *ArXiv Astrophysics e-prints*
Nelson, L. A., Rappaport, S. A., and Joss, P. C.: 1986, *Astrophysical Journal* **304**, 231
Palm, D.: 2011, *The Astronomer's Telegram* 3663
Peterson, C. J. and King, I. R.: 1975, *Astronomical Journal* **80**, 427
Prodan, S. and Murray, N.: 2015, *Astrophysical Journal* **798**, 117
Remillard, R. A. and Levine, A. M.: 2008, *The Astronomer's Telegram* 1853
Ricci, C., Beckmann, V., Carmona, A., and Weidenspointner, G.: 2008, *The Astronomer's*

Telegram 1840
Ryden, B.: 2016, *Dynamics:*, Ohio State Graduate Astrophysics Series, Office of Distance Ed & eLearning at OSU
Savonije, G. J., de Kool, M., and van den Heuvel, E. P. J.: 1986, *A&A* **155**, 51
Seward, F. D. and Charles, P. A.: 1995, *Exploring the X-Ray Universe*
Shakura, N. I. and Sunyaev, R. A.: 1973, *A&A* **24**, 337
Sidoli, L., La Palombara, N., Oosterbroek, T., and Parmar, A. N.: 2005, *A&A* **443**, 223
Spruit, H. C.: 2010, *ArXiv e-prints*
Strohmayer, T. and Bildsten, L.: 2003, *ArXiv Astrophysics e-prints*
Swank, J. H., Becker, R. H., Pravdo, S. H., Saba, J. R., and Serlemitsos, P. J.: 1976, *IAU Cirulars* 3010
Wiersema, K., Russell, D. M., Degenaar, N., Klein-Wolt, M., Wijnands, R., Heinz, S., Read, A. M., Saxton, R. D., and Tanvir, N. R.: 2009, *Monthly Notices of the RAS* **397**, L6
Worpel, H., Galloway, D. K., and Price, D. J.: 2013, *Astrophysical Journal* **772**, 94
Yoon, D., Morsony, B., Heinz, S., Wiersema, K., Fender, R. P., Russell, D. M., and Sunyaev, R.: 2011, *Astrophysical Journal* **742**, 25
Zhong, J. and Wang, Z.: 2011, *Astrophysical Journal* **729**, 8